

GENERALIZED SYSTEM IDENTIFICATION WITH STABLE SPLINE KERNELS

ALEKSANDR Y. ARAVKIN*, JAMES V. BURKE†, AND GIANLUIGI PILLONETTO ‡

Abstract. Regularized least-squares approaches have been successfully applied to linear system identification. Recent approaches use quadratic penalty terms on the unknown impulse response defined by *stable spline kernels*, which control model space complexity by leveraging regularity and bounded-input bounded-output stability. This paper extends linear system identification to a wide class of nonsmooth stable spline estimators, where regularization functionals and data misfits can be selected from a rich set of piecewise linear quadratic penalties. This class encompasses the 1-norm, huber, and vaponik, in addition to the least-squares penalty, and the approach allows linear inequality constraints on the unknown impulse response.

We develop a customized interior point solver for the entire class of proposed formulations. By representing penalties through their conjugates, we allow a simple interface that enables the user to specify any piecewise linear quadratic penalty for misfit and regularizer, together with inequality constraints on the response. The solver is locally quadratically convergent, with $O(n^2(m+n))$ arithmetic operations per iteration, for n impulse response coefficients and m output measurements. In the system identification context, where $n \ll m$, IPsolve is competitive with available alternatives, illustrated by a comparison with TFOCS and libSVM.

The modeling framework is illustrated with a range of numerical experiments, featuring robust formulations for contaminated data, relaxation systems, and nonnegativity and unimodality constraints on the impulse response. Incorporating constraints yields significant improvements in system identification. The solver used to obtain the results is distributed via an open source code repository.

Keywords: linear system identification; kernel-based regularization; Gaussian processes; bias-variance; model order selection; robust statistics; sparse optimization; interior point methods

1. Introduction. System identification formalizes the pervasive process of inferring models from observations and studying their properties. A *system*, broadly speaking, is an object in which variables of different kinds interact to produce observable signals [52]. This abstraction applies to a wide range of scientific phenomena, including heating of buildings, ship-steering dynamics, speech, electric circuits, and biological processes.

A key concept in modeling real-world systems is *model selection*. Specifying a viable model space is essential to finding a good model fit for given observed inputs and outputs. We focus on *time invariant linear* system (LTI) identification, i.e. systems where the response to a certain input signal does not depend on absolute time, and where the output response to a linear combination of inputs is precisely the linear combination of the responses to individual inputs. This class is computationally tractable, and has been successful in a wide range of applications including NMR spectroscopy, seismology, circuits, signal processing, control theory, biological processes, and many others.

Within the class of LTI systems, model selection and model space exploration remains a key concept. The general workflow of system identification proceeds as follows: (i) select a set of candidate models that increase in complexity (ii) fit each model to observed data and (iii) find the ‘best’ model using a complexity measure. For LTI systems, the classic approach builds parametric models of different orders using autoregressive models with exogenous inputs (ARX) or autoregressive moving average models with exogenous inputs (ARMAX). These models are typically fit to data using Prediction Error Methods (PEM) based on quadratic penalties [52, 77]. The “best” model is selected using a variety of complexity measures such as Akaike information criterion (AIC), Bayesian information criterion (BIC) or by cross validation (CV) techniques [2, 75, 38].

This standard approach has a number of limitations [65, 67]. For example, when the number

*Applied Mathematics Department, University of Washington, Seattle, WA, (saravkin@uw.edu). Research was supported by the Washington Research Foundation Fund for Innovation in Data-Intensive Discovery.

†Mathematics Dept., University of Washington, Seattle, WA 98195 (burke@math.washington.edu).

‡Control and Dynamic Systems Department of Information Engineering at the University of Padova, Padova, Italy (giapi@dei.unipd.it)

November 8, 2022

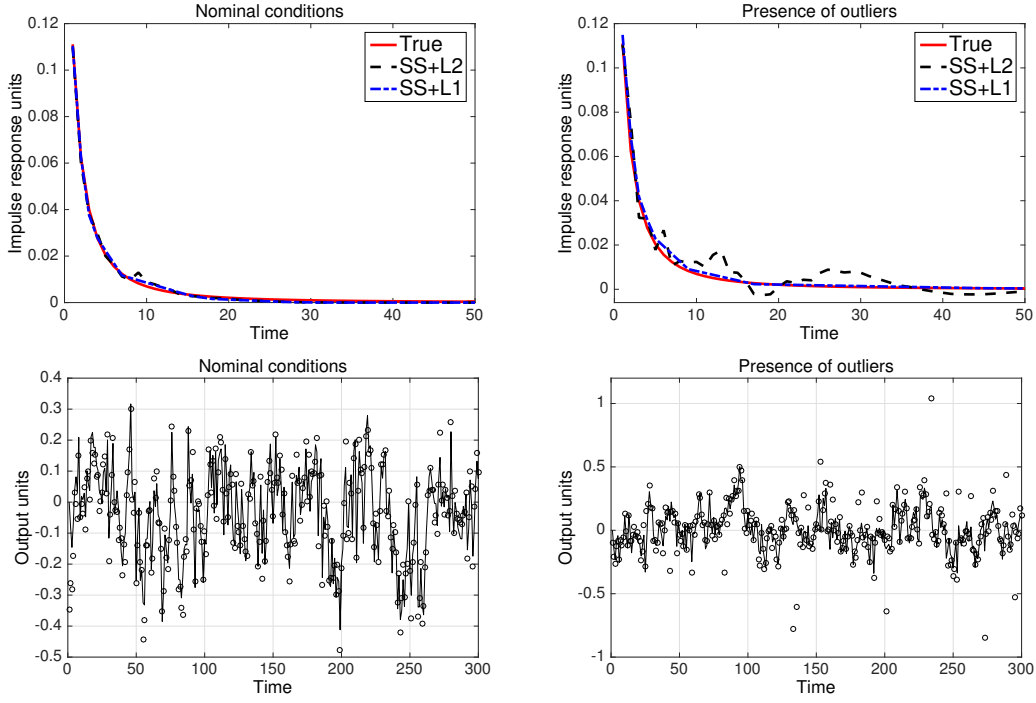


Fig. 1.1: Introductory example. *Top*: true impulse response (red solid) and estimates obtained under nominal conditions (left) and in presence of outliers (right) using the stable spline estimator (Section 2.3) with L_2 loss (black dash) and L_1 loss (blue dash-dot). *Bottom*: linearly interpolated noiseless outputs (solid line), and noisy measurements (\circ) under nominal conditions (left) and in presence of outliers (right).

of available output measurements is relatively small (so that asymptotic theory underlying AIC is not applicable), the selected models often have poor predictive capability on new data. In some cases, identifying a system is a highly ill-conditioned inverse problem [12], and principled regularization techniques are required for estimate estimation. In addition, the classical approach cannot incorporate additional information about the system, including domain restrictions, monotonicity, and unimodality; this information may be crucial, as it can significantly narrow the focus of the search, and dramatically improve estimation. Finally, reliance on least-squares leaves the system identification process vulnerable to model misspecification, such as outliers in the observations (that are poorly modeled by the Gaussian distribution) [41, 31, 4, 29].

Illustrative example. Some of the drawbacks to the standard approach are illustrated by the example in Fig. 1.1 (implementation details are given in Appendix 7.1). The impulse response (top panels, solid red line) is estimated from noisy outputs obtained using white noise as system input. Consider two different situations. In the first case, the data set of 1000 samples is corrupted by white stationary Gaussian noise (bottom left panel). The estimate obtained using the stable spline estimator (discussed in Section 2.3) using the L_2 loss (top left, black dashdot line) is close to the true signal. In the second case, the data set is corrupted by a few of outliers (bottom right panel). Now, the impulse response profile (top right panel, black dashdot line) reveals the vulnerability of the L_2 loss to deviations in the noise model.

Contributions. In this paper, we build a broad new modeling framework for model exploration in LTI system identification, together with a custom solver for all formulations. The modeler can choose from a range of convex *piecewise linear-quadratic (PLQ)* penalties that make system identification robust to outliers. We incorporate regularization into this framework, leveraging the recently developed *stable spline kernel* approach to control model space complexity. Finally, we show how to incorporate constraints on the signal response, allowing the modeler to significantly narrow the search when additional information is available. All of these extensions are implemented in an open source solver IPSolve¹. In the remaining portion of the introduction, we give a brief survey of each component of the proposed framework.

Piecewise linear-quadratic penalties (PLQ). The limitations of the quadratic loss motivate the use of alternative losses that are robust to outliers, including the L_1 -norm, the Huber loss [41], the Vapnik ε -insensitive [81, 69] and the hinge loss [28, 73] (the last two penalties are used for support vector regression and classification). All of these penalties fall into the PLQ class, and appear in Figures 3.1a-3.1i. Just as the L_2 penalty corresponds to maximum likelihood estimation with Gaussian errors, other penalties can be viewed as negative log likelihoods for non Gaussian noise [32]. For instance, the L_1 loss corresponds to assuming the noise follows a particular generalization of the Laplacian distributions [4], and analogous likelihood interpretations have been developed for Vapnik and Huber penalties [9].

Stable-spline kernels. Recent approaches cast system identification as a kernel learning problem, formulated in a Hilbert space [65, 64, 68]. Ill-posedness and ill-conditioning are studied within a Gaussian regression framework [70]. The unknown impulse response is modeled as a Gaussian process whose covariance encodes available prior knowledge, and estimators proposed in [65, 63] model covariances using *stable spline kernels*, which include information on regularity and exponential stability of the impulse response. Extensive simulation studies have shown that stable spline estimators have advantages over the classical approach, especially in terms of the quality of the model complexity selection. [68] presents an overview of these new techniques and their relationship to machine learning.

General regularizers. Though quadratic penalization of stable spline coefficients has proved to be effective, other choices can yield dramatic improvements. For example, if the impulse response is expected to have many zero entries, the inclusion of a sparsity promoting prior can significantly improve the quality of the estimator, e.g. the Laplace prior, or L_1 loss, used in the LASSO [79]. This leads to a weighted combination of norms in the spirit of the elastic net procedure [87]. Our framework includes these priors, allowing any PLQ penalty to be used for regularization (see Figures 3.1a-3.1i).

Incorporating constraints. In many situations, additional system information can be incorporated using inequality constraints on the impulse response coefficients. For instance, nonnegativity is often a consequence of physical considerations. In addition, relaxed systems are frequently encountered in real-world applications — examples include reciprocal electrical networks and mechanical systems with negligible inertial phenomena. The peculiarity of these systems is that their impulse response is a completely monotonic function [82] (also, see (5.2) in Section 5). The impulse response in Fig. 1.1 is one example, and it corresponds to a function that never exhibits oscillations. Other interesting cases arise in biomedicine. For instance, in bolus-tracking magnetic resonance imaging (MRI) [86] quantification of cerebral hemodynamics requires estimation of impulse responses known to be positive and unimodal. In all of these examples, there is a wealth of prior knowledge about the signal, and one expects that incorporating this knowledge into system identification will yield significant improvements. These expectations are borne out, see Figures 5.1 and 5.3.

¹<https://github.com/saravkin/IPsolve>

Custom solver. Convex optimization has become a standard tool in many applications, and general convex solvers such as the MATLAB package CVX [34] and TFOCS [10] are important tools for prototyping and testing new ideas. However, these general tools are not competitive with solvers that exploit problem-specific structure. IPSolve strikes a good balance between generality and exploiting problem structure; outperforming TFOCS in the system identification context. For large-scale system identification problems that can be formulated as support vector regression (SVR), IPSolve is competitive with the libSVM [17] solver. These examples are developed in section 5.2.

We extend prior general work in PLQ modeling and optimization [7, 9] by incorporating inequality constraints, and develop convergence guarantees for the entire framework in Theorem 4.3. We then apply the constrained PLQ framework to the linear system identification scenario, and compare resulting estimators with classical PEM and stable spline approaches in a range of numerical studies, featuring contaminated data, and the inclusion of additional information about the impulse response, e.g. unimodality or complete monotonicity.

Road map. The structure of the paper is as follows. In Section 2, we review the classical approach to linear system identification, and provide a brief introduction to the stable spline estimation technique. In Section 3, we formulate the general class of nonsmooth stable spline estimators, using PLQ penalties as misfits and regularizers, and incorporate inequality constraints on the impulse response. We then show in Section 4 how interior point methods that exploit special PLQ representations can efficiently compute the impulse response estimates. In Section 5, we compare against TFOCS and libSVM to illustrate scaling and efficiency of IPSolve, and also test the performance of new estimators using several Monte Carlo studies, including estimators for the example discussed in the introduction. We end the paper with Conclusions, and include additional proofs and information regarding numerical experiments in the Appendix.

2. PEM and stable spline approaches to linear system identification. In this section, we review the classic PEM approach to system identification, and contrast it with an approach to controlling model complexity via stable-spline kernels.

2.1. Statement of the problem. Consider the following linear time-invariant discrete-time system

$$y(t) = G(q)u(t) + e(t) \quad (2.1)$$

where y is the output, q is the shift operator $qu(t) = u(t+1)$, $G(q)$ is the linear operator associated with the true system, which is assumed stable, u is the input, and e is white noise with variance σ^2 .

Our problem is to estimate the system impulse response assuming that the system input is known for m measurements of y at instants $t = 1, \dots, m$. We then measure the quality of an estimator \hat{G} by means of the fit measure

$$\mathcal{F}(G, \hat{G}) = 100 \left(1 - \frac{\|G - \hat{G}\|_2}{\|G\|_2} \right) \quad (2.2)$$

where, given a linear system $S(q)$, $\|S\|_2$ is the L_2 -norm of its impulse response.

2.2. Classical linear system identification. A general parametrized model space \mathcal{M} , with parameter x , for linear systems is given by parametrizing the transfer function G from input to output:

$$z(t) = G(q, x)u(t) + e(t). \quad (2.3)$$

For instance, a standard *black box* description assumes G is a rational function of the shift operator q ,

$$G(q, x) = \frac{B(q)}{C(q)} \quad (2.4)$$

where $B(q)$ and $C(q)$ are polynomials in q^{-1} whose unknown coefficients are the components of x . Different model structures can be associated with different degrees of $B(q)$ and $C(q)$. For each model structure, the parameters x can be estimated by PEM [52], i.e.

$$\hat{x} = \underset{x}{\operatorname{argmin}} V(x), \quad (2.5)$$

where V is often a quadratic loss:

$$V(x) = \sum_{t=1}^m (z(t) - G(q, x)u(t))^2. \quad (2.6)$$

In real applications, a suitable model structure (dimension of x) is typically unknown and needs to be inferred from data. This step is crucial, as it balances bias and variance to reach a good impulse response reconstruction. Popular approaches include cross validation [38], Akaike's criterion [2], and its small-sample version, corrected Akaike's criterion (AICc) [42].

2.3. The stable spline estimator. A drawback to rational transfer functions is that they require solving (2.5), a nonconvex and potentially high-dimensional problem, for each postulated model order. A common alternative is the FIR-model obtained setting $C(q) = 1$ in (2.4), which makes (2.5) a linear least-squares problem in the polynomial coefficients x for B :

$$\begin{aligned} V(x) &= \sum_{t=1}^m (z(t) - B_x(q)u(t))^2 \\ &= \sum_{t=1}^m (z_t - \langle \phi(u_t, q), x \rangle)^2, \end{aligned} \quad (2.7)$$

where $\phi(u_t, q)$ is a vector determined by the input and shift operators. However, a high-order FIR, often necessary to capture system dynamics, can suffer from high variance, so regularization is crucial.

We quickly review the regularized approaches described in [65, 19]. First rewrite the measurement model (2.7) using matrix-vector notation:

$$z = \Phi x + E, \quad (2.8)$$

where $z \in \mathbb{R}^m$ is a vector comprising the m output measurements, Φ is a matrix with rows $\phi_t = \phi(u_t, q)$ determined by input values and shift operator, E is the noise, and $x \in \mathbb{R}^n$ is the (column) vector of impulse response coefficients. In contrast to classical approaches to system identification, the n th-order FIR approach does not need to balance bias and variance, but only needs to be of sufficiently large order to capture the system dynamics. Here, the model complexity is controlled via stable spline kernels. A stable spline estimator for impulse response solves

$$\hat{x} = \underset{x}{\operatorname{argmin}} \|z - \Phi x\|^2 + \gamma x^T Q^{-1} x, \quad (2.9)$$

where the positive scalar γ is the *regularization parameter*, while $Q \in \mathbb{R}^{n \times n}$ is a regularization matrix defined by the class of the stable spline kernels [63]. Problem (2.9) is always well-posed because of the strongly convex term $\gamma x^T Q^{-1} x$, which also controls model order. When

using the discrete-time version of the first-order stable spline kernel (also called TC kernel in [19]), the (i, j) entry of Q is specified to be

$$Q_{ij} := \alpha^{\max(i,j)}, \quad \text{for some } 0 \leq \alpha < 1. \quad (2.10)$$

Smoother impulse response estimates can be obtained by using the second-order stable spline kernel. In this case, the entries of Q are given by

$$Q_{ij} := \left[\frac{\alpha^{(i+j)} \alpha^{\max(i,j)}}{2} - \frac{\alpha^{3\max(i,j)}}{6} \right], \quad \text{for some } 0 \leq \alpha < 1. \quad (2.11)$$

In (2.10) and (2.11), α is a kernel hyperparameter related to the dominant pole of the system (i.e. it establishes how fast the impulse response decays to zero) and is typically unknown. See [66] and [18] for a discussion of the merits of the stable spline kernels under both a Bayesian and a deterministic perspective.

Stable spline kernels depend on two unknown hyperparameters; specifically the estimator (2.9), where Q is given by (2.10) or (2.11), depends on α and γ , which need to be determined from data. This can be accomplished by marginal likelihood maximization [57, 53, 11, 7, 6]. We detail the hyperparameter estimation procedure in Section 5.

Learning hyperparameters is analogous to model order selection in the classical PEM framework. Once the two parameters are found, the impulse response estimate for the least-squares formulation can be obtained by solving a linear system of equations given by the first-order optimality conditions for the problem (2.9).

3. New formulations of the stable spline estimator. We now introduce the class of piecewise linear quadratic (PLQ) functions and penalties. We first develop a representation calculus for estimators of interest using simple PLQ building blocks, and then show how to formulate general estimation problems as minimizers of a single PLQ objective over a polyhedral set. All estimators can then be obtained using the solution procedure developed in Section 4. We conclude this section by providing the details on how to construct the associated PLQ function in three important cases: (i) L_1 regression with an L_2 regularizer, (ii) Support vector regression with an L_2 regularizer, and (iii) L_2 regression with an ‘elastic net’ regularizer.

3.1. From quadratic to PLQ penalties. It is useful to rewrite the estimator (2.9) as:

$$y = L^{-1}x, \quad Q = LL^T \quad (3.1)$$

where L is invertible thanks to the positive definite property of stable spline kernels (we caution that the variable y introduced here is *not* the same object as the function $y(t)$ defined in (2.1)). In the new variable y the estimation problem (2.9) translates into the problem

$$\min_y \|z - \Phi Ly\|^2 + \gamma \|y\|^2. \quad (3.2)$$

This estimator uses quadratic functions for both the misfit penalty and the regularizer. The goal of the remainder of the paper is to show how to generalize (3.2) for adaptation to a variety of data scenarios and to illustrate the computational efficacy of these adaptations.

Let Y denote the feasible polyhedral constraint region for y . Then an explicit representation for Y can be written as

$$Y = \{y : A^T y \leq a\}, \quad A \in \mathbb{R}^{n \times p}, \quad a \in \mathbb{R}^p. \quad (3.3)$$

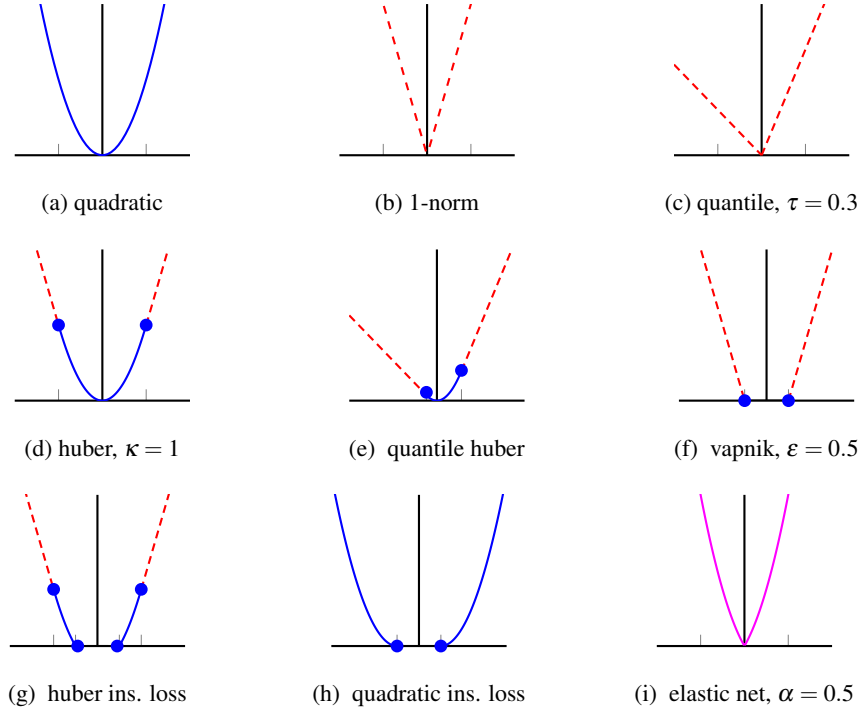


Fig. 3.1: Important piecewise linear-quadratic (PLQ) losses.

This allows us to represent prior knowledge about the signal, including domain information (e.g. lower and upper limits), as well as monotonicity or unimodality properties.

We consider generalizations of (3.2) that use any PLQ penalty:

$$\min_{y \in Y} V(z - \Phi L y) + \gamma W(y), \quad (3.4)$$

where V and W are piecewise linear quadratic functions introduced below, and Y is as in (3.3). Nine important examples of these penalties appear in Figures 3.1a-3.1i.

DEFINITION 3.1 (PLQ functions and penalties). *A piecewise linear quadratic (PLQ) function is any function $\rho(c, C, b, B, M; \cdot) : \mathbb{R}^n \rightarrow \overline{\mathbb{R}}$ admitting representation*

$$\rho(c, C, b, B, M; y) = \sup_{u \in U} \left\{ \langle u, b + B y \rangle - \frac{1}{2} \langle u, M u \rangle \right\}, \quad (3.5)$$

where U is the polyhedral set specified by $C \in \mathbb{R}^{k \times \ell}$ and $c \in \mathbb{R}^k$ as follows

$$U = \{u : C^T u \leq c\}, \quad (3.6)$$

$M \in \mathcal{S}_+^k$ is the set of real symmetric positive semidefinite matrices, $b + B y$ is an injective affine transformation in y , with $B \in \mathbb{R}^{k \times n}$, so, in particular, $n \leq k$ and $\text{null}(B) = \{0\}$. If $0 \in U$, then the PLQ is necessarily non-negative and hence represents a penalty.

Below we show that the nine loss functions illustrated in Figures 3.1a-3.1i are members of the PLQ class. In the following section, it is shown how this *dual*, or *conjugate*, representation

for the PLQ class facilitates the development of algorithms for their optimization. Our use of the terms dual and conjugate stem from the fact that the representation (3.5) defines ρ in terms of its *convex conjugate* [71].

Examples of scalar PLQ

- (a) The least-squares penalty (Fig. 3.1a) is ubiquitous in linear and nonlinear regression [30, 76] and inverse problems [80]:

$$\frac{1}{2}x^2 = \sup_u \left\{ ux - \frac{1}{2}u^2 \right\}.$$

- (b) The use of the 1-norm (Fig. 3.1b) as a regularizer appears in a numerous applications, including machine learning and compressed sensing [37, 27, 25], image denoising [78, 54, 55], and seismic image processing [40, 59, 39, 56]:

$$\|x\|_1 = \sup_{u \in [-1, 1]} \{ux\}.$$

- (c) The quantile (τ) penalty (Fig. 3.1c, $\tau = 0.3$), an asymmetric generalization of the 1-norm, is used to analyze heterogeneous datasets [44, 14] in computational biology [89], survival analysis [45], and economics [46, 43]:

$$q_\tau(x) = \sup_{u \in [-\tau, (1-\tau)]} \{ux\}.$$

- (d) The huber function (Fig. 3.1d) is used in robust regression settings [41, 58, 13, 26, 21, 51]:

$$h_\kappa(x) = \sup_{u \in [-\kappa, \kappa]} \left\{ ux - \frac{1}{2}u^2 \right\}.$$

- (e) The quantile huber (Fig. 3.1e) was recently introduced in [1] and shown to have superior performance to the quantile penalty in the high-dimensional setting. It can be obtained by smoothing the quantile loss (Fig. 3.1c):

$$h_{\tau, \kappa}(x) = \sup_{u \in [-\kappa\tau, \kappa(1-\tau)]} \left\{ ux - \frac{1}{2}u^2 \right\}.$$

- (f) The Vapnik penalty (Fig. 3.1f) is used in support vector regression (SVR) [81, 38, 73, 74] and functional recovery [5]:

$$\rho_\varepsilon(x) = \sup_{u \in [0, 1]^2} \left\{ \left\langle \begin{bmatrix} 1 \\ -1 \end{bmatrix} x - \begin{bmatrix} \varepsilon \\ \varepsilon \end{bmatrix}, u \right\rangle \right\}$$

- (g) (Huberized) smooth insensitive loss (Fig. 3.1g) has been a popular penalty for support vector regression [20, 48, 24]:

$$\rho_\varepsilon^h(x) = \sup_{u \in [0, 1]^2} \left\{ \left\langle \begin{bmatrix} 1 \\ -1 \end{bmatrix} x - \begin{bmatrix} \varepsilon \\ \varepsilon \end{bmatrix}, u \right\rangle - \frac{1}{2}u^T u \right\}.$$

- (h) The (quadratic) smooth loss (Fig. 3.1h) has also been used for SVR [49], and is obtained by relaxing U from $[0, 1]^2$ to \mathbb{R}_+^2 :

$$\rho_\varepsilon^q(x) = \sup_{u \in \mathbb{R}_+^2} \left\{ \left\langle \begin{bmatrix} 1 \\ -1 \end{bmatrix} x - \begin{bmatrix} \varepsilon \\ \varepsilon \end{bmatrix}, u \right\rangle - \frac{1}{2} u^T u \right\}$$

- (i) The elastic net penalty (Fig. 3.1i) has been widely used for sparse regularization with correlated predictors [88, 87, 50, 23]. It is obtained by a linear combination of the 1-norm and quadratic loss:

$$\rho(x) = \sup_{u \in [0, 1] \times \mathbb{R}} \left\{ \left\langle \begin{bmatrix} 1 \\ 1 \end{bmatrix} x, u \right\rangle - \frac{1}{2} u^T \begin{bmatrix} 0 & 0 \\ 0 & 1 \end{bmatrix} u \right\}.$$

the set U is shown explicitly, but in each case can be easily represented as $U := \{u : C^T u \leq c\}$.

The conjugate representation in Definition 3.1 is used to establish a computational framework for solving our generalized linear system identification problem (3.4). It is important to note that PLQ functions can be added and composed with linear maps, and that conjugate representations of these generalized objects can be obtained from the representation of the component parts. The following remarks give two of the most important tools in PLQ representational calculus.

REMARK 3.1 (Affine composition). *Take any PLQ function $\rho(c, C, b, B, M; y)$. Suppose that $y = Ex + e$, where $x \mapsto Ex + e$ is an injective affine transformation in x . Then we have*

$$\rho(c, C, b, B, M; Ex + e) = \rho(c, C, b + Be, BE, M; x)$$

so the composition is also a PLQ function, with representation $c, C, b + Be, BE, M$.

REMARK 3.2 (PLQ addition). *Given two PLQ functions $\rho(c_1, C_1, b_1, B_1, M_1; y)$ and $\rho(c_2, C_2, b_2, B_2, M_2; y)$, the sum is also a PLQ function, with representation*

$$c = \begin{bmatrix} c_1 \\ c_2 \end{bmatrix}, C = \begin{bmatrix} C_1 & 0 \\ 0 & C_2 \end{bmatrix}, b = \begin{bmatrix} b_1 \\ b_2 \end{bmatrix}, B = \begin{bmatrix} B_1 \\ B_2 \end{bmatrix}, M = \begin{bmatrix} M_1 & 0 \\ 0 & M_2 \end{bmatrix}.$$

These remarks show that the PLQ class is closed under addition and affine composition, allowing the design of a PLQ penalty that is well suited to a given application. For given PLQ penalties V and W , their sum (3.4) is also a PLQ penalty, with a representation that can be automatically constructed from individual components using the above remarks. Once a representation for (3.4) is constructed, we show, in the next section, that it can be optimized over any polyhedral set.

3.2. Estimation by PLQ Optimization. As noted in the previous section, when V and W are PLQ functions, the problem (3.4) can be formulated as a problem of the form

$$\begin{aligned} \min_y \quad & \rho(c, C, b, B, M; y) \\ \text{s.t.} \quad & A^T y \leq a, \end{aligned} \tag{3.7}$$

for an appropriate choice of ρ as in (3.5, 3.6). To illustrate the power of this result, we formulate three estimators of the form (3.4) using well established PLQ penalties. In each case, we give the explicit characterization of (3.4) in terms of its reformulation $\rho(\cdot; y)$ in (3.7). These characterizations are obtained using the examples in Section 3, together with the calculus presented in Remarks 3.1 and 3.2.

Examples of estimators of form (3.4)

1. If $V = \|\cdot\|_1$ and $W = \|\cdot\|_2^2$, the problem (3.4) can be written in the form (3.7) by setting

$$c = \begin{bmatrix} \mathbf{1} \\ \mathbf{1} \\ 1 \end{bmatrix}, C = \begin{bmatrix} I & \\ & -I \\ & & 0 \end{bmatrix}, b = \begin{bmatrix} -z \\ 0 \end{bmatrix}, B = \begin{bmatrix} \Phi L \\ I \end{bmatrix}, M = \begin{bmatrix} 0 & 0 \\ 0 & \frac{1}{2\gamma} I \end{bmatrix}$$

($u \in \mathbb{R}^n$ is represented by the single constraint $0^T u \leq 1$).

2. If V is the Vapnik function with parameter ε and $W = \|\cdot\|_2^2$, as in the previous example, then problem (3.4) can be written in the form (3.7) by setting

$$c = \begin{bmatrix} \mathbf{1}\kappa \\ \mathbf{0}\kappa \\ \mathbf{1}\kappa \\ \mathbf{0}\kappa \\ 1 \end{bmatrix}, C = \begin{bmatrix} I & \\ -I & \\ I & \\ -I & \\ & 0 \end{bmatrix}, b = \begin{bmatrix} -\varepsilon\mathbf{1} - z \\ -\varepsilon\mathbf{1} + z \\ 0 \end{bmatrix},$$

$$B = \begin{bmatrix} \Phi L \\ -\Phi L \\ I \end{bmatrix}, M = \begin{bmatrix} 0 & 0 & 0 \\ 0 & 0 & 0 \\ 0 & 0 & \frac{1}{2\gamma} I \end{bmatrix}.$$

3. Let $V = \frac{1}{2}\|\cdot\|_2^2$ and $W(y) = \frac{\gamma_1}{2}\|y\|^2 + \gamma_2\|Ly\|_1$. This specifies an ‘elastic net’ prior on y , i.e. a weighted combination of a quadratic and an absolute value loss. In this case, problem(3.4) can be written in the form (3.7) by setting

$$c = \begin{bmatrix} 1 \\ 1 \\ \gamma_2\mathbf{1} \\ \gamma_2\mathbf{1} \end{bmatrix}, C = \begin{bmatrix} 0 & & & \\ & 0 & & \\ & & I & \\ & & & -I \end{bmatrix}, b = \begin{bmatrix} -z \\ 0 \end{bmatrix},$$

$$B = \begin{bmatrix} \Phi L \\ I \\ L \end{bmatrix}, M = \begin{bmatrix} I & 0 & 0 \\ 0 & \frac{1}{\gamma_1} I & 0 \\ 0 & 0 & 0 \end{bmatrix}.$$

4. An Interior Point (IP) Approach. We now show how to solve (3.7) using interior point IP methods [47, 60, 84]. IP methods solve nonsmooth optimization problems by applying a damped Newton method to a homotopy path that parametrizes the underlying Karush-Kuhn-Tucker (KKT) system. In this regard, the first key observation is that the KKT system for (3.7) is an instance of a *monotone mixed linear complementarity problem* (MLCP) [84] since it can be written as

$$\begin{pmatrix} s \\ r \\ 0 \\ 0 \end{pmatrix} = \left[\begin{array}{cc|cc} 0 & 0 & -C^T & 0 \\ 0 & 0 & 0 & -A^T \\ \hline C & 0 & M & -B \\ 0 & A & B^T & 0 \end{array} \right] \begin{pmatrix} q \\ w \\ u \\ y \end{pmatrix} + \begin{pmatrix} c \\ a \\ b \\ 0 \end{pmatrix} \quad (4.1)$$

with

$$0 \leq \begin{pmatrix} q \\ w \end{pmatrix}, \begin{pmatrix} s \\ r \end{pmatrix} \text{ and } \begin{pmatrix} q \\ w \end{pmatrix}^T \begin{pmatrix} s \\ r \end{pmatrix} = 0, \quad (4.2)$$

where the matrix in (4.1) is positive semi-definite (see Appendix for details). Consequently, it is possible to transform this MLCP into a monotone LCP and solve it by an interior point

algorithm [47]. However, this transformation is arduous, especially in high dimensions, and may be prohibitively expensive [3, 36, 83]. In [83] it is noted that the transformation to an LCP is not essential if the matrix

$$\mathcal{H} := \begin{bmatrix} -C^T & 0 \\ 0 & -A^T \\ M & -B \\ B^T & 0 \end{bmatrix} \in \mathbb{R}^{(\ell+p+k+n) \times (k+n)} \quad (4.3)$$

is injective. In our context, the injectivity of this matrix can be established under mild conditions.

THEOREM 4.1 (Injectivity of \mathcal{H}). *Suppose $M \in \mathcal{S}_+^k$ and $B \in \mathbb{R}^{k \times n}$ is such that $\text{null}(B) = \{0\}$. Then the matrix \mathcal{H} in (4.3) is injective if and only if*

$$\text{Nul}(M) \cap \text{Nul}(B^T) \cap \text{Nul}(C^T) = \{0\}. \quad (4.4)$$

Condition (4.4) is satisfied if the stronger condition

$$\text{Nul}(M) \cap \text{Nul}(B^T) = \{0\} \quad (4.5)$$

holds. This latter condition is satisfied by all of the PLQ functions described in Sections 3.1 and 3.2 [9, 8].

As first step toward the statement of the algorithm, we precisely define all of the quantities appearing in (3.7). Let

$$\begin{aligned} b &\in \mathbb{R}^k, C \in \mathbb{R}^{k \times l}, c \in \mathbb{R}^l, B \in \mathbb{R}^{k \times n}, \\ A &\in \mathbb{R}^{n \times p}, M \in \mathbb{R}^{k \times k}, \text{ and } a \in \mathbb{R}^p, \end{aligned} \quad (4.6)$$

and set $N := 2l + 2p + k + n$. Then, given $\mu \geq 0$, define $F_\mu : \mathbb{R}^N \rightarrow \mathbb{R}^N$ by

$$F_\mu(q, w, u, y, s, r) := \begin{pmatrix} C^T u + s - c \\ A^T y + r - a \\ Mu + Cq - By - b \\ B^T u + Aw \\ Qs - \mu \mathbf{1} \\ Wr - \mu \mathbf{1} \end{pmatrix}, \quad (4.7)$$

where $Q := \text{diag}(q)$ and $W := \text{diag}(w)$. By setting $\mu = 0$, the KKT conditions (4.1)-(4.2) can equivalently be written as

$$F_\mu(q, w, u, y, s, r) = 0 \text{ for } s, q \in \mathbb{R}_+^l \text{ and } r, w \in \mathbb{R}_+^p, \quad (4.8)$$

where the variables $y \in \mathbb{R}^n$ and $u \in \mathbb{R}^k$ are those that appear in the definition of the PLQ function ρ (3.5). Variables s and r (called slack variables) are defined to satisfy

$$r = a - A^T y \geq 0, \quad s = c - C^T u \geq 0.$$

The variables q and w are the dual variables that correspond to these constraints $C^T u \leq c$ and $A^T y \leq a$, respectively. For future reference, we make the following definitions: for any positive integer ℓ set $\mathbb{R}_+^\ell := \{x \in \mathbb{R}^\ell : 0 \leq x_i, i = 1, 2, \dots, \ell\}$ and denote the interior of \mathbb{R}_+^ℓ by \mathbb{R}_{++}^ℓ .

An interior point approach applies a damped Newton iteration to a relaxed version of the KKT system by solving (4.8) for $\mu > 0$ and letting μ carefully descend to zero. This is accomplished by choosing an initial $(y^0, u^0) \in \mathbb{R}^n \times \mathbb{R}^k$ and $(s^0, r^0, q^0, w^0) \in \mathcal{D}_{++}$ where $\mathcal{D}_{++} :=$

$\mathbb{R}_{++}^l \times \mathbb{R}_{++}^p \times \mathbb{R}_{++}^l \times \mathbb{R}_{++}^p$, and then preserving the positivity of the iterates (s^v, r^v, q^v, w^v) at each iteration of the damped Newton method for (4.8). For this to succeed, the Newton iteration must be well-defined, that is, for $\mu > 0$ a unique solution to

$$F_\mu((q, w, u, y, s, r)^k) + F_\mu^{(1)}((q, w, u, y, s, r)^k) \left((q, w, u, y, s, r) - (q, w, u, y, s, r)^k \right) = 0$$

must exist. That is, $F_\mu^{(1)}$ must be invertible at all iterates. On \mathcal{D}_{++} , we have

$$F_\mu^{(1)}(q, w, u, y, s, r) = \left[\begin{array}{cc|cc|cc} 0 & 0 & -C^T & 0 & -I & 0 \\ 0 & 0 & 0 & -A^T & 0 & -I \\ \hline C & 0 & M & -B & 0 & 0 \\ 0 & A & B^T & 0 & 0 & 0 \\ \hline Q & 0 & 0 & 0 & S & 0 \\ 0 & W & 0 & 0 & 0 & R \end{array} \right], \quad (4.9)$$

where $S = \text{diag}(s)$ and $R = \text{diag}(r)$. We now show that the invertibility of $F_\mu^{(1)}$ is related to the condition (4.4) in Theorem 4.1.

THEOREM 4.2 (Invertibility of $F_\mu^{(1)}$). *Given $(u, y) \in \mathbb{R}^k \times \mathbb{R}^n$ and $(q, w, s, r) \in \mathcal{D}_{++}$, the matrix $F_\mu^{(1)}(q, w, u, y, s, r)$ is invertible if and only if the matrix*

$$\begin{bmatrix} M + CSQ^{-1}C^T & -B \\ B^T & ARW^{-1}A^T \end{bmatrix} \quad (4.10)$$

is invertible, which, in turn, is equivalent to condition (4.4).

Note that the central 2×2 block of $F_\mu^{(1)}(q, w, u, y, s, r)$ is precisely the block matrix appearing in the lower right of the MLCP matrix (4.1), and Theorem 4.2 relates (4.4) to the algebraic implementation of the interior point method for the general problem (3.7), which we now outline.

ALGORITHM 4.1. *Interior Point Method for (3.4).*

Inputs:

- $y^0 \in \mathbb{R}^n, u^0 \in \mathbb{R}^k$: *initial primal variables*
- $s^0 \in \mathbb{R}_{++}^l, r^0 \in \mathbb{R}_{++}^p$: *initial positive slack estimates*
- $q^0 \in \mathbb{R}_{++}^l, w \in \mathbb{R}_{++}^p$: *initial positive dual variables*
- $0 \leq \mu^0$: *initial relaxation parameter*
- $0 < \eta < 1$: *line search parameter*

Iteration:

1. *Set the iteration counter $v = 0$, and label*
 $\chi = [q^T \ w^T \ u^T \ y^T \ s^T \ r^T]^T$.
2. *(Relaxed Newton Step:)*
Find $d = [d_q^T \ d_w^T \ d_u^T \ d_y^T \ d_s^T \ d_r^T]^T$ such that

$$F_\mu^{(1)} d = -F_\mu.$$

3. (Line Search) Set

$$\begin{aligned}
t_v &= \max \gamma^i \\
\text{s.t. } & i \in \{0, 1, 2, \dots\}, \\
& \begin{bmatrix} s^v + t_v d_s \\ r^v + t_v d_r \\ q^v + t_v d_q \\ w^v + t_v d_w \end{bmatrix} > 0, \text{ and} \\
& \|F_v(\chi^v + \gamma^i d^v)\| \leq (1 - \eta) \|F_v(\chi^v)\|
\end{aligned}$$

4. (χ -update) Set

$$\chi^{v+1} = \chi^v + t_v d^v$$

5. (μ -update) Set

$$\mu^{v+1} = \frac{1}{p+l} ((s^{v+1})^T q^{v+1} + (r^{v+1})^T w^{v+1})$$

6. (Iterate) Set $v = v + 1$ and return to Step 2.

The convergence analysis for the interior point algorithm relies on the following sets: let $\tau > 0$ and define

$$\mathcal{F}_+(\tau) := \left\{ (q, w, u, y, r, s) \left| \begin{array}{l} (u, y) \in \mathbb{R}^k \times \mathbb{R}^n, (q, w, s, r) \in \mathcal{D}_{++} \\ \text{and equation (4.1) is satisfied} \\ \text{with } q^T s + w^T r \leq \tau \end{array} \right. \right\}$$

and $\mathcal{C} := \{(q, w, u, y, r, s) \mid (4.8) \text{ holds for some } \mu > 0\}$.

The set \mathcal{C} is called the *central path*. The key to the complexity analysis for the algorithm is to ensure that the iterates hew sufficiently close to this path as μ descends to zero.

THEOREM 4.3 (Convergence Properties). *Consider any optimization problem of the form (3.7) satisfying (4.6). If $\mathcal{F}_+(+\infty) \neq \emptyset$ and (4.4) holds, then Algorithm 4.1 is implementable, the sets $\mathcal{F}_+(\tau)$ are non-empty, convex, and bounded for all $\tau > 0$, the central path is well-defined, and every cluster point of the central path as $\mu \downarrow 0$ is a KKT point for (3.7).*

The proof of this result appears in the appendix. The details for computing the Newton step (Step (2)) when (4.5) is satisfied are also given in the Appendix where it is shown that the matrices

$$T := M + CSQ^{-1}C^T \text{ and } \Omega := B^T T^{-1} B + ARW^{-1}A^T, \quad (4.11)$$

and their inverses, play a key role. The matrix T is invertible since (4.5) holds, and Ω is invertible since T is invertible and B is injective. The sparsity of these matrices determine the complexity of the algorithm since the computation of the Newton step is the major effort at each iteration. Note that in our examples of PLQ functions the matrices M and C are very sparse; indeed, the matrix T is always diagonal. The next result describes the per iteration complexity of the algorithm assuming that T is diagonal.

THEOREM 4.4 (PLQ Iteration Complexity). *If the matrices $T_k := M + CS_k Q_k^{-1} C^T$ in Algorithm 4.1 are diagonal, then every interior point iteration can be computed with complexity $O(n^2(k + p + n))$.*

The assumptions on the structure of M and C that yield a diagonal T are satisfied by many common PLQ penalties. For example, for L_2 we have $M = I$ and $C = 0$, for L_1 and the Vapnik penalty, $M = 0$ and C contains two copies of the identity matrix.

Turning our attention back to system identification, n is the dimension of the impulse response, while k and l depend on m , in particular $k \geq m$, while l depends on the structure of the PLQ penalties used to build the estimate (3.4).

COROLLARY 4.5 (SysID Iteration Complexity). *If the constraint matrix A contains $O(n)$ entries (as e.g. with box constraints), while matrices B and C have on the order of m entries, each interior point iteration can be solved with complexity $O(n^2(m+n))$.*

The above result shows that IP computational complexity scales favorably with the number of measurements m which, in system identification, is typically much larger than the number of unknown impulse response coefficients n .

5. Numerical studies. The power of the new approach is illustrated by three numerical studies. In subsection 5.1, our introductory example replaces the quadratic data misfit with robust losses (L_1 and Vapnik) to guard against outliers. Here, our framework is used to design an estimator that incorporates prior knowledge that data come from a relaxation system. The resulting fit illustrates the remarkable regularizing effect of complete monotonicity constraints on the impulse response.

In subsection 5.2, we compare the approach to two competing alternatives, the general first-order package TFOCS [10] and optimized SVM and SVR package libSVM [17]. The approach, implemented in the package IPSolve, is faster than TFOCS on every example, and beats libSVM on many large scale problems; it is important to keep in mind that $n \ll m$ in the system identification context.

In subsection 5.3, we study robustness of new PLQ stable spline estimators with respect to outliers via a Monte Carlo study. In addition, we compare the performance of the new methods to *ideal* PEM and SS estimators that use an oracle to tune the model hyperparameters to achieve the best fit based on the measure $\mathcal{F}(G, \hat{G})$ defined in (2.2). While these ideal estimators are not implementable in practice, the comparison is illuminating, especially for the new estimators that include constraints.

Finally, subsection 5.4 uses simulated realistic magnetic resonance imaging data, featuring a scenario where impulse response is known to be unimodal. These results further illustrate how system identification performance is greatly enhanced by means of impulse response constraints, outperforming PEM estimators tuned with an oracle.

5.1. Introductory example: robust estimation with inequality constraints . Results in Fig. 1.1 illustrate the well established fact that the estimator $SS + L_2$ based on the quadratic loss is vulnerable to outliers (recall that SS refers to stable spline in Section 2.3). Here we exploit the general framework of the previous section to design a robust estimator by replacing the quadratic (Gaussian) with the absolute value (Laplace) loss. This leads to the estimator $SS + L_1$ defined by

$$\hat{x} = \arg \min_x \|z - \Phi x\|_1 + \gamma x^T Q^{-1} x. \quad (5.1)$$

This objective can be transformed into form (3.4) and then into (3.7) using example (1) in Section 3.2. As in the quadratic case (2.9), the solution depends on the unknown parameters γ and α (which enters Q). To solve (5.1), γ and α are estimated via cross validation, splitting the data into a training and a validation set of equal size. The “optimal” hyperparameters values are obtained by searching over a two dimensional grid. In particular, α and γ assume values on the grid defined, respectively, by the MATLAB commands

```
A=[0.01 0.05:0.05:0.95 0.99],
B=logspace(log10(g/100), log10(g*100), 50),
```

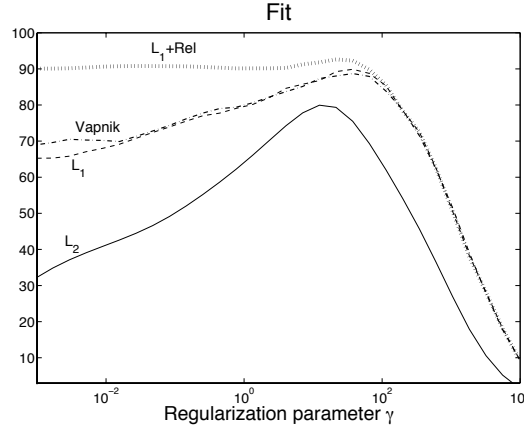


Fig. 5.1: Introductory example. Fit, as a function of the regularization parameter γ , obtained using the stable estimator equipped with the L_2 , L_1 and Vapnik loss, and combining the L_1 loss with the information that data come from a relaxation system ($L_1 + Rel$).

with σ set to the value of γ adopted by $SS + L_2$.

The top panels of Fig. 1.1 display the impulse response estimates obtained by $SS + L_1$ (dashed line). The advantage of the new robust formulation is evident. While $SS + L_1$ and $SS + L_2$ exhibit a similar performance under nominal conditions (top left panel), $SS + L_1$ outperforms $SS + L_2$ in presence of outliers (top right panel), returning an impulse response estimate much close to truth. The robustness of the L_1 loss w.r.t. large model deviations is due to the fact that it pushes some residuals to zero. It thus detects which measurements are more accurate, essentially treating them as constraints during the fitting.

To further compare $SS + L_2$ and $SS + L_1$, Fig. 5.1 plots the fit (2.2) returned by these two estimators as a function of the regularization parameter γ (with α constant, fixed to its estimate). The figure reveals that the adoption of the quadratic loss makes it difficult to choose the regularization parameter: many values of γ lead to poor estimates, e.g. $\gamma \leq 1$ leads to outliers overfitting. On the other hand the fit profile associated with $SS + L_1$ is more stable, and is uniformly better than $SS + L_2$.

We have also tested the Vapnik loss formulation of the stable spline estimator. This objective can be written in form (3.7) using example (2) in Section 3.2. The fit profile is displayed in Fig. 5.1 (parameters α and ε are constant, set to their cross validated estimates) and is similar to the one obtained by $SS + L_1$. Even though it requires estimation of the additional parameter ε , an advantage of the Vapnik loss over the L_1 is its data compression capability: it detects the so called support vectors which contain those measurements influencing the estimate, see [37] for details.

The last estimator tested embodies the information that the data come from a relaxation system. This means that the impulse response is a completely monotonic function (e.g. see Section 4 in [22]) and, hence, its derivatives $f^{(\ell)}$ satisfy

$$(-1)^\ell f^{(\ell)}(t) \geq 0, \quad t \geq 0, \quad \ell = 0, 1, \dots \quad (5.2)$$

Since $x = Ly$, in discrete-time this information is (approximately) encoded in (3.7) by setting a to the null vector and

$$A^T = \begin{bmatrix} -I_n \\ D^1 \\ -D^2 \\ \vdots \\ (-1)^{k-1} D^k \end{bmatrix} L,$$

with k a sufficiently large integer and D an $n \times n$ lower triangular Toeplitz matrix whose first column is $[1, -1, 0, \dots]^T$. Let $SS + Rel$ denote the estimator (5.1) complemented with the above constraints ($k = 5$), with the parameter α set to the estimate used by $SS + L_1$. The corresponding fit is reported in Fig. 5.1: $SS + Rel$ shows impressive performance for a wide range of regularization parameter values. Interestingly, the model incorporating the complete monotonicity constraint competes favorably with the overfit residuals even for very low values of γ . This example illustrates the observation that the inclusion of additional model information in the form of constraints often helps to regularize the estimation process while simultaneously improving the fit.

5.2. Computational efficiency: comparison of IPSolve, TFOCS and libSVM. In this section, we compare the computational efficiency of the IPSolve approach with those of two widely used publicly available packages, TFOCS [10] and libSVM [17]. While in fields such as machine learning it is often assumed that the number of unknowns is much larger than the data set size $m \gg n$, in system identification it is typically assumed that $n \gg m$. This makes the per iteration complexity $O(n^2(m+n))$ of our algorithm (see Corollary 4.5) particularly appealing. We illustrate the advantages with a numerical comparison in this setting, for the specific problem

$$\arg \min_x \|z - \Phi x\|_\varepsilon + \gamma x^T Q^{-1} x, \quad (5.3)$$

where $\|\cdot\|_\varepsilon$ denotes the Vapnik loss (Fig. 3.1f), with noisy data z generated from the impulse response used in the introductory example (Fig. 1.1, top panel). The objective is specified using parameters $\gamma = 10$, $\alpha = 0.5$ in (2.10), and $\varepsilon = 0.1$.

5.2.1. TFOCS. The TFOCS algorithm [10] is based on the proximal point algorithm, and can be applied to generic convex minimization problems. The TFOCS software² can handle a broader class of problems than IPSolve (i.e. problems that are not piecewise linear quadratic). The relevant standard form for TFOCS is the problem

$$\min \phi(x) = f(x) + \frac{\mu}{2} \|x - x_0\|^2 + h(\mathcal{A}(x) - b), \quad (5.4)$$

where the proximity operator for both f and h can be efficiently computed. In particular, applying TFOCS to (5.3) requires a proximity operator for the Vapnik penalty; i.e. a routine that solves

$$p_\varepsilon(x) = \arg \min_y \frac{1}{2} \|x - y\|^2 + \|y\|_\varepsilon.$$

TFOCS combines dual smoothing techniques with optimal first-order methods [10, 61, 62] and is therefore capable of solving large-scale problems (much larger than those that can be solved with other general convex solvers, such as the MATLAB package CVX [34, 35]). Like IPSolve, it is a general purpose software that can be used to solve (5.3).

²<http://cvxr.com/tfocs>

5.2.2. libSVM. libSVM is an optimization package³ aimed at support vector problems, including problems of type 5.3. It uses pre-compiled routines with several interfaces, including one for Matlab. libSVM is designed for a broad range of support vector problems, including kernel machines; for our problem of interest, the formulation available through libSVM is a slight modification of (5.3):

$$\arg \min_{x,b} \|z - \Phi x - b\mathbf{1}\|_\varepsilon + \gamma x^T Q^{-1} x \quad (5.5)$$

The inclusion of intercept b is not optional for libSVM; we therefore compared libSVM with IPSolve on (5.5).

libSVM solves the *dual* problem to (5.5):

$$\begin{aligned} \min_{\alpha \in \frac{1}{\gamma} \mathbb{B}_\infty} \quad & \frac{1}{2} \alpha^T (Q^{T/2} \Phi^T \Phi Q^{1/2}) \alpha + \varepsilon \|\alpha\|_1 + \langle z, \alpha \rangle. \\ \text{s.t.} \quad & \mathbf{1}^T \alpha = 0. \end{aligned} \quad (5.6)$$

This is a quadratic problem, and libSVM solves it using a specialized decomposition approach. By focusing on the dual, libSVM is able to handle linear and nonlinear SVM and SVR; it has been widely applied in practice.

In the system identification context, however, we have $n \ll m$; and as shown in Corollary 4.5, the number of arithmetic operations required to implement each iteration is $O(n^2(n+m))$. In contrast, a naive approach for solving (5.6) requires $O(m^3)$ operations. While the approach of [17] is far from naive, it is optimized for kernel machines, where one must restrict all computation to the m -dimensional dual (since the primal dimension may be infinite); in contrast IPSolve exploits the structure of the problem, performing most computations for (5.3) in an n -dimensional space.

5.2.3. Experimental setup and results. We compare all three approaches for problem (5.3) using $n \in \{100, 150, 200, 250, 300\}$ and $m \in \{1000, 2000, 5000, 10000, 20000\}$. The scales of (m, n) are chosen to reflect the system identification context, where $n \ll m$. We run each algorithm until their available optimality criteria fall below $\varepsilon = 10^{-6}$; The precise criteria are different for all three algorithms:

- IPSolve uses a relative magnitude of the Karush-Kuhn-Tucker system; it terminates when

$$\frac{\|F_{\text{current}}\|}{\|F_{\text{initial}}\|} < \varepsilon,$$

for $F = F_0$ in (4.7).

- TFOCS allows the user to select one of several stopping criterias; some are based on optimality of problem (5.4); but there is also a relative criteria based on iterate convergence,

$$\frac{\|x_{k+1} - x_k\|}{\max(1, \|x_{k+1}\|)} < \varepsilon$$

that allows the algorithm to terminate early. This is the criteria we selected; internal optimality criteria required a far larger number of iterations, during which the objective value did not change significantly. To optimize performance of TFOCS,

³<https://www.csie.ntu.edu.tw/~cjlin/libsvm/>

$\frac{m}{n}$	1K	2K	5K	10K	20K	$\frac{m}{n}$	1K	2K	5K	10K	20K
100	0.376	0.730	1.333	2.666	5.365	100	3.320	5.292	5.815	10.896	20.483
150	0.426	0.886	2.782	4.225	7.862	150	4.882	4.196	6.800	11.194	26.349
200	0.464	1.149	3.040	4.796	10.105	200	3.545	3.985	9.282	10.710	32.644
250	0.464	1.273	3.541	6.176	11.463	250	3.840	5.167	8.722	14.787	30.289
300	0.715	1.633	3.966	7.418	13.773	300	3.256	4.471	6.787	11.186	17.403

$\frac{m}{n}$	1K	2K	5K	10K	20K
100	0.0418	0.0046	0.0024	0.0044	0.0022
150	0.0179	0.0080	0.0015	0.0068	0.0260
200	0.0175	0.0135	0.0053	0.0055	0.0399
250	0.0074	0.0055	0.0028	0.0208	0.0100
300	0.1423	0.1424	0.1756	0.0982	0.1748

Table 5.1: Top tables: CPU time (seconds) taken by IPsolve (left) and TFOCS (right) to solve (5.3) as a function of the dimension n of x and of the data set size m . Bottom table: relative (signed) objective difference of the solutions. IPsolve *always* gets the lower objective value; and it is uniformly faster for all problems tested. Note that TFOCS is very accurate.

we experimented with choice of first-order solvers, but found the default algorithm (Auslender & Teboulle’s single-projection method) to be the best. We also tuned the ‘restart’ option to restart the step-length computation every 1000 iterations; as this improved performance of TFOCS, as recommended by the authors.

- libSVM convergence criteria for the SVR problem, as explained in [17], is based on the iterate α satisfying a KKT criteria for (5.6) within ε (in the infinity norm).

In summary, we have two similar optimization problems, (5.3) and (5.5), and three sets of convergence criteria. To fairly compare the algorithms, we run IPsolve against TFOCS on problem (5.3), and IPsolve against libSVM on problem (5.5). In each case, we tabulate both timing results, and also show an ‘accuracy’ heuristic, which is the signed *relative objective difference* (ROD):

$$\text{ROD}(*) := \frac{f_{(*)} - f_{\text{IPsolve}}}{f_{\text{IPsolve}}}$$

A positive ROD indicates IPsolve found the lower objective value; a relative scale is chosen because we consider a range of problem sizes.

Results of the numerical study are shown in Tables 5.1 and 5.2. IPsolve gets uniformly better objective values for all experiments, and performs faster than TFOCS for all problem sizes. Notably, TFOCS is very accurate at the settings we compared, with all ROD values less than 10^{-5} .

libSVM is more competitive in its timing, but also less accurate, with some ROD values exceed 10^{-2} , i.e. libSVM primal values are more than 1% larger than those of IPsolve on some of the problems. Overall, IPsolve converges faster for approximately half of the problems; it especially has an advantage for large m and small n as expected. It should be noted that libSVM has strange behavior for the $n = 300$ case; it converges very quickly, but the solutions are less accurate than for other problems.

5.3. Monte Carlo study in the presence of outliers. We now consider a Monte Carlo study of 1000 sample runs. For each run, a random single-input single-output (SISO) con-

$\begin{smallmatrix} m \\ \backslash \\ n \end{smallmatrix}$	1K	2K	5K	10K	20K	$\begin{smallmatrix} m \\ \backslash \\ n \end{smallmatrix}$	1K	2K	5K	10K	20K
100	0.293	0.629	1.303	2.427	5.011	100	0.764	0.343	2.305	8.528	32.944
150	0.421	0.791	2.061	4.197	7.522	150	0.124	0.485	2.930	11.628	46.038
200	0.504	1.111	2.791	4.827	9.040	200	0.153	0.586	3.691	14.909	59.223
250	0.621	1.148	3.263	6.086	10.460	250	0.161	0.667	4.348	17.885	72.330
300	0.719	1.271	3.865	7.314	13.077	300	0.052	0.107	0.450	1.515	5.330

$\begin{smallmatrix} m \\ \backslash \\ n \end{smallmatrix}$	1K	2K	5K	10K	20K
100	1.8080	0.2988	0.0284	0.1225	0.0037
150	1.4702	0.1488	0.0241	0.0997	0.0049
200	3.5449	0.1984	0.0172	0.1130	0.0004
250	1.5892	0.1723	0.0141	0.1643	0.0080
300	5.4052	21.9701	3.8528	0.4366	1.2052

Table 5.2: Top tables: CPU time (seconds) taken by IPSolve (left) and libSVM (right) to solve (5.5) as a function of the dimension n of x and of the data set size m . Bottom table: relative (signed) objective difference of the solutions. Note that IPSolve *always* gets the lower objective value, and it is faster for the majority of the problems. Note also that libSVM is a lot less accurate than TFOCS (accuracy measured by IPSolve objective).

	$Oe+Or$	$SS+Or$	$Oe+CV$	$SS+CV$	$SS+ML$
L_2 loss	64.31	68.9	-303.2	59.7	63.1
L_1 loss	79.9	82.3	-73.1	71.8	72.8

Table 5.3: Monte Carlo study (subsection 5.3). Average fit achieved by the PEM and stable spline estimators using the L_2 and the L_1 loss.

tinuous time model of order 30 is generated and then sampled at three times its bandwidth. The Matlab code is given below:

```
m=rss(30); b=bandwidth(m); f = b*3*2*pi;
md=c2d(m,1/f,'zoh'); md.d = 0;
```

The command `c2d` converts a continuous-time dynamic system to discrete time, while `md.d` is the feedforward matrix of the the sampled model. We accept only models with all poles in a disk of radius 0.95 in the complex plane. The model `md`, initially at rest, is given a Gaussian white noise input with unit variance filtered by a randomly generated model obtained by the same process already described. The input delay is always equal to 1. We then generate 1000 measurements contaminated by outliers, and use them to reconstruct the impulse response. The measurement errors are a mixture of two normals given by $e_i \sim 0.7\mathcal{N}(0, \sigma^2) + 0.3\mathcal{N}(0, 100\sigma^2)$, with σ^2 equal to the variance of the noiseless output divided by 100. Thus, with probability 0.3, a measurement becomes an ‘outlier’, since the corresponding simulated error has standard deviation 10σ .

We compare the performance of five different estimators over the 1000 runs of the simulation. Each estimator uses either quadratic or 1-norm loss for data fidelity, and all formulations treat the system input delay and initial conditions as known. The estimators are enumerated below.

- $Oe+Or$ is the classical PEM approach (MATLAB command `oe`), and we compare

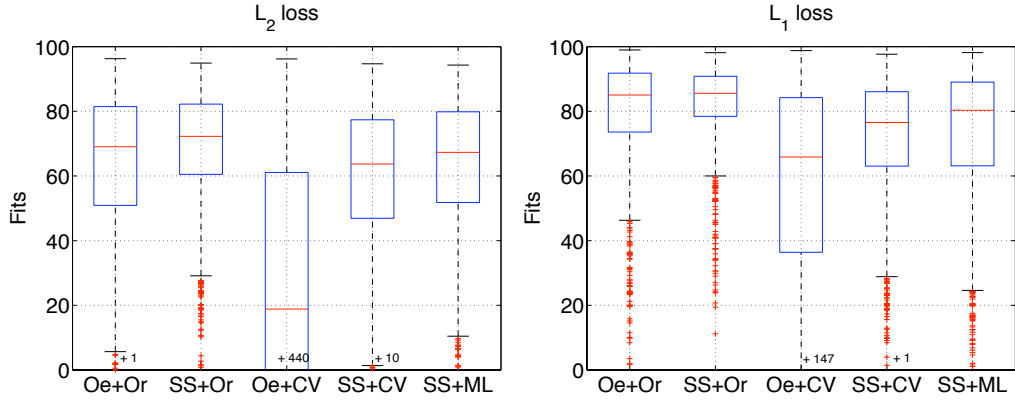


Fig. 5.2: Monte Carlo study (subsection 5.3). Boxplot of the 1000 percentage fit measures (2.2) obtained by PEM and stable spline estimators equipped with the L_2 loss (left panel) and the L_1 loss (right panel).

the quadratic loss (2.6) with the 1-norm loss⁴

$$V(x) = \sum_{t=1}^m |y(t) - G(q, x)u(t)|.$$

Candidate models are rational transfer functions (2.4) with polynomials B and C of the same order. The estimator is not implementable in practice, since it makes use of an oracle which selects the model order maximizing the percentage fit measure (2.2). The purpose of the use of an oracle in the simulation is to provide a baseline for comparison with the *best achievable* PEM performance when the optimal model order is known.

- *Oe+CV* is an implementable analogue of *Oe+Or* that uses cross-validation to estimate model order. Data are split into training and validation sets of equal size. For every model order ranging from 1 to 30, a model is trained using command `oe` on the training set. We then choose the order that minimizes the sum of squared prediction errors on the validation set, obtained by using the command `predict` with null initial conditions. Once the order is found, the final model is computed by `oe` using all measurements in training and validation sets.
- *SS+Or* is the stable spline estimator using the stable spline kernel (2.10). Again, we compute the fit using both the quadratic loss (2.9) and the 1-norm loss (5.1) for the purpose of comparison. The number of estimated impulse response coefficients is 200, i.e. $\dim(x) = 200$. This estimator also uses an oracle which gives values for the hyperparameters α and γ that maximize the percentage fit measure (2.2). As is the case for *Oe+Or*, this method is not implementable, but provides a baseline for the *best possible* performance of a stable spline estimator.
- *SS+ML* is an implementable analogue of *SS+Or* that uses marginal likelihood maximization to estimate hyperparameters. The procedure depends on the choice of loss function (quadratic or 1-norm).

For the quadratic loss, α , γ and σ^2 are estimated using the following procedure.

⁴The robust PEM method has been implemented exploiting the option (`'LimitError'`, r) with $r = 1e - 20$.

1. Estimate σ^2 (the noise variance) by fitting a low-bias FIR model of order p , (see e.g. in [33] for details), and then set

$$\hat{\sigma}^2 = \frac{\sum_{t=1}^m (y(t) - \hat{G}(q)u(t))^2}{m-p}, \quad (5.7)$$

where \hat{G} is the p th-order FIR obtained by least-squares.

2. We use the model (2.8) to estimate of α and γ by applying the following Bayesian interpretation of (2.9). Let E and x be independent Gaussian vectors with covariances $\sigma^2 I_m$ and λQ , respectively, where I_m is the $m \times m$ identity matrix and λ is a positive scalar. Then, for $\gamma = \sigma^2 / \lambda$, \hat{x} is the minimum variance estimate of the impulse response, and so λ and α can be estimated by maximizing the *marginal likelihood* obtained by integrating x out of the joint density for (x, z) :

$$(\hat{\lambda}, \hat{\alpha}) = \arg \min_{\lambda, \alpha} \{z^T \Sigma^{-1} z + \log \det(\Sigma)\}, \quad \Sigma := \lambda \Phi Q \Phi^T + \hat{\sigma}^2 I_m. \quad (5.8)$$

Then let $\hat{Q} = Q(\hat{\alpha})$ and $\hat{\Sigma} = \Sigma(\hat{\lambda}, \hat{\alpha})$ be the estimates of Q and Σ with $\lambda = \hat{\lambda}$ and $\alpha = \hat{\alpha}$. From (2.9), the final impulse response estimate becomes

$$\hat{x} = \hat{\lambda} \hat{Q} \Phi^T \hat{\Sigma}^{-1} z. \quad (5.9)$$

For the 1-norm loss, we model components of E in (2.8) as independent Laplacian random variables with variance σ^2 . Hence, for known hyperparameters, the negative log posterior of x given z is given by

$$\sqrt{\frac{2}{\sigma^2}} \|z - \Phi x\|_1 + \frac{1}{2\lambda} x^T Q^{-1} x$$

with constant terms omitted. Then (5.1) is the MAP estimator of x given z if

$$\gamma = \frac{\sigma^2}{2\sqrt{2\lambda}}. \quad (5.10)$$

However, under the Laplacian assumption, estimation of λ and α via marginal likelihood is an analytically intractable problem. A simple yet effective heuristic is to take λ and α to be the same estimates as obtained under Gaussian noise assumptions (i.e. optimizing (5.8)), then using (5.10) and (2.10) to obtain γ and Q , respectively.

- **SS+CV** is nearly identical to **SS+ML**, but with hyperparameters estimated by cross-validation. Data are split into a training and validation set of equal size and the best values of γ and α are found over a two dimensional grid. Specifically, the α - γ grid is $A \times B$, where the sets A and B are given by the MATLAB commands:

```
A=[0.01 0.05:0.05:0.95 0.99]
B=logspace(log10(g/100), log10(g*100), 50),
```

with g taken to be the value of γ used in **SS+ML**.

The plots in Fig. 5.2 show Matlab boxplots of the 1000 percentage fit measures (2.2) obtained by the five estimators. The rectangle contains the inter-quartile range (25 – 75% percentiles) of the fits, with median shown with a red line. The “whiskers” outside the rectangle display the upper and lower bounds of all the numbers, not counting what are deemed outliers, plotted separately as “+”. Table 5.3 also reports the average percentage fit values.

The left panel of Fig. 5.2 shows the fits achieved by the quadratic estimators. Oracle-based

procedures highlight the advantage of the stable spline estimators: $SS+Or$ shows better performance than $Oe+Or$. The performance gap increases in implementable estimators, when hyperparameters are learned from data (as necessary in practical situations). $SS+CV$ and $SS+ML$ have similar performance, and both are much better than $Oe+CV$.

The right panel of Fig. 5.2 displays the fits achieved by all five estimators when using the 1-norm data fidelity loss function. These estimators are more robust against outliers, and all fits improve significantly. Furthermore, as in the previous case, performance of stable spline estimators is superior to that of the classical system identification procedures.

5.4. Assessment of cerebral hemodynamics using magnetic resonance imaging. The quantitative assessment of the cerebral blood flow is essential to the understanding of brain function. For this purpose, an important technique is bolus-tracking magnetic resonance imaging (MRI), which relies on established principles for tracer kinetics of nondiffusible tracers [86]. These principles allow for the quantification of cerebral hemodynamics by solving a linear system identification problem. In this scenario, the system output is the measured tracer concentration within a given tissue volume of interest, while the system input is the measured arterial function. The impulse response is proportional to the so called *tissue residue function*, and is known to be positive and unimodal. It carries fundamental information on the system under study, e.g. the cerebral blood flow is given by its maximum value. However, impulse response estimation is especially difficult for this problem: even if the noise can be reasonably modeled as Gaussian, the problem is often ill-conditioned and only a few noisy output samples are available [85].

We consider realistic simulation studies, using four different types of estimators all based on the quadratic loss. The first two rely on the classical PEM paradigm. They are $Oe+Or$, described in the previous subsection, with the maximum allowed model order equal to 10, and $Oe+AICc$, which uses the AICc criterion [42] for model complexity selection. $SS+ML$ uses the stable spline kernel (2.11), estimates hyperparameters via marginal likelihood optimization, and then uses (2.9) to find the final impulse response, where $x \in \mathbb{R}^{100}$. The last estimator $SS+ML+um$ also estimates hyperparameters via marginal likelihood optimization, and then incorporates nonnegativity and unimodality information. Specifically, we minimize objective (2.9) (with hyperparameter estimates identical to those used by $SS+ML$), subject to *inequality constraints* that impose unimodality:

$$\begin{cases} D_1^k x_1^k & \geq 0 \\ D_{k+1}^n x_{k+1}^n & \leq 0 \\ x & \geq 0. \end{cases} \quad (5.11)$$

Here, $D \in \mathbb{R}^{n \times n}$ is the discrete derivative operator, i.e. a lower triangular Toeplitz matrix with first column $[1, -1, 0, \dots]^T$, D_1^k and D_{k+1}^n contain, respectively, the first k and the last $n-k$ rows of D , and analogously for x_1^k and x_{k+1}^n . In terms of (3.7), this is specified setting a to the null vector and

$$A^T = \begin{bmatrix} -D_1^k \\ D_{k+1}^n \\ -I_n \end{bmatrix} L. \quad (5.12)$$

We solve the problem for each k , obtaining a set of solutions $\hat{x}(k)$, and then select the best \bar{k} for (2.9) by setting

$$\bar{k} = \arg \min_k \|z - \Phi \hat{x}(k)\|^2 + \gamma(\hat{x}(k))^T Q^{-1} \hat{x}(k),$$

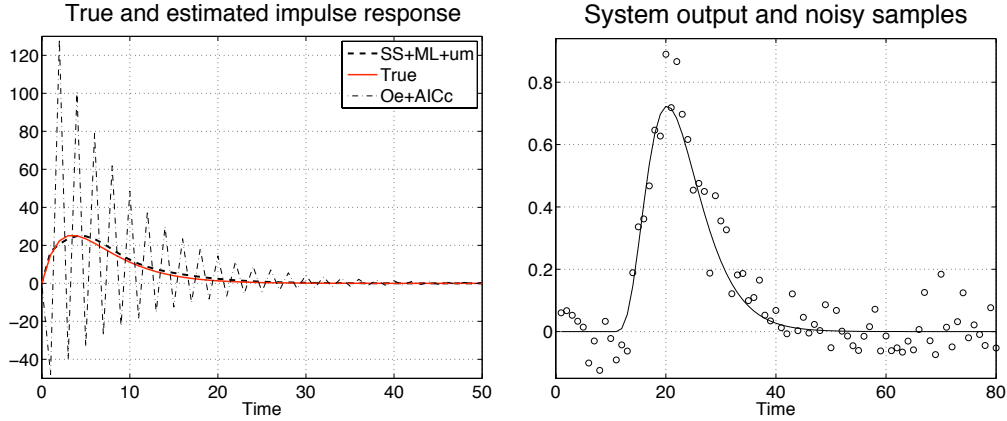


Fig. 5.3: Assessment of cerebral hemodynamics using magnetic resonance imaging. The left panel shows the true impulse response (solid line), the estimate by PEM with AICc to select the model order (dashdot line) and the estimate by the stable spline estimator incorporating unimodality constraints (dashed line). The right panel displays the noiseless output (solid line) and the measurements (\circ).

with the final estimator given by $\hat{x}(\bar{k})$, the best unimodal estimator. We begin by considering the simulation described in [85]. The system input is the typical arterial function $u(t) = (t - 10)^3 e^{-\frac{2t}{3}}$ if $t > 10$ and zero otherwise, while the impulse response is the dispersed exponential displayed in Fig. 5.3 (left panel, solid line). This response is to be reconstructed from the 80 noisy output samples reported in Fig. 5.3 (right panel). These measurements are generated as detailed in subsection II.A of [85], using parameters typical of a normal subject with a signal to noise ratio equal to 20 and discretizing the problem using unit sampling instants.

The left panel of Fig. 5.3 shows the estimate by $Oe+AICc$ (dashdot). It is apparent that the reconstructed profile is far from the true one and contains many non-physiological oscillations: the asymptotic theory underlying AICc does not compensate for ill-conditioning. The same panel also displays the estimate from $SS+ML+um$ (dashed line). This estimate is very close to truth, outlining the importance of regularization and the inclusion of additional information in the form of constraints when handling these data poor situations. This result is confirmed by a Monte Carlo study of 1000 runs where independent noise realizations are generated at every run. Fig. 5.4 shows the Matlab boxplots of the 1000 percentage fit measures (2.2) achieved by the four estimators in the reconstruction of the impulse response (left panel) and of its peak (right panel). Most of the time $Oe+AICc$ returns negative fits, while the outcomes from $Oe+Or$ and $SS+ML$ are similar with good performance (keep in mind $Oe+Or$ is not implementable in practice). Finally, notice that $SS+ML+um$ has the best performance vis-à-vis the percentage fit measures (2.2), see also Table 5.4 for the average fits.

6. Conclusions. This paper extends stable spline estimators to allow general modeling of misfit measures, regularizers, and constraints. Quadratic losses and regularizers can now be replaced by general PLQ functions. Furthermore, affine inequality constraints on the unknown impulse response can also be incorporated, providing a simple mechanism for the inclusion of information on domain restriction, monotonicity, and unimodality of the signal. We have seen how this can have a profound impact on the quality of the recovery and can sig-

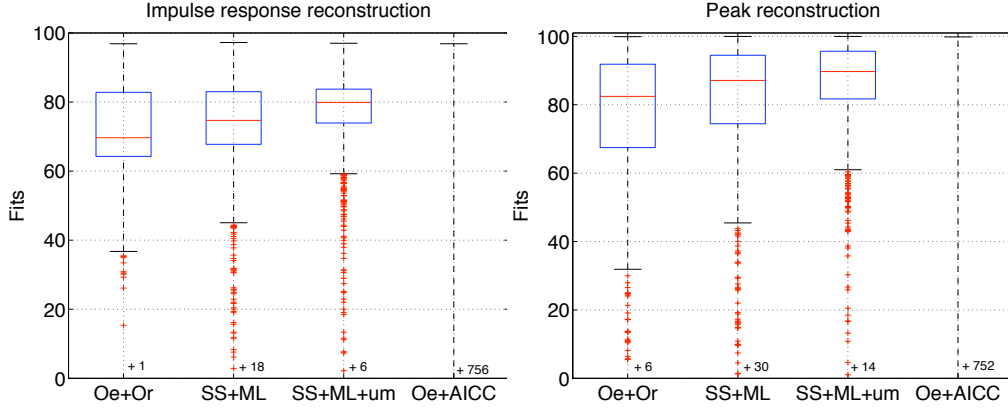


Fig. 5.4: Assessment of cerebral hemodynamics using magnetic resonance imaging. Box-plot of the 1000 percentage fit measures (2.2) for the impulse response reconstruction (left) and peak reconstruction (right) obtained by PEM equipped with an oracle and with AICc for model order selection, by the stable spline estimator and by the stable spline estimator incorporating unimodality constraints.

	<i>Oe+Or</i>	<i>SS+ML</i>	<i>SS+ML+um</i>	<i>Oe+AICc</i>
Imp. response	71.9	69.8	76.3	-3497.1
Peak	77.1	76.2	84.3	-26.3

Table 5.4: Average percentage fit (2.2) achieved by the PEM and stable spline estimators relative to impulse response and peak reconstruction.

nificantly improve the fit when a regularizing prior is required for identification (as illustrated in Fig. 5.1).

The new framework allows the user to formulate and explore a vast number of new system identification procedures, e.g. by balancing robustness against outliers, introducing sparsity promoting priors, or introducing additional model information by means of affine inequality constraints.

All of the extensions have been implemented in the open source package IPSolve. Numerical comparisons in Section 5.2 showed that for system identification, IPSolve outperforms competing alternatives, including both TFOCS and libSVM; this is explained by the $O(n^2(n+m))$ arithmetic operations per iteration in a context where $n \ll m$.

The examples gathered in the paper illustrate the power of this new kernel-based framework in comparison to the classical approaches used in the literature. An important example comprises impulse responses known to be positively or completely monotonic, in the presence of outliers. Classic approaches (using PEM and rational transfer function models (2.4)) solve a non-convex (and possibly non-differentiable) high-dimensional inequality constrained optimization problem ($\dim(x)$ specifies domain complexity) *for each postulated model structure*. Model order selection, a delicate issue even in the unconstrained case, becomes, *a fortiori*, even harder. These drawbacks have greatly limited the use of algorithms for inequality constrained/non-smooth linear system identification.

In contrast, using the kernel-based approach developed here, instead of working with a high dimensional vector x , we consider only a low-dimensional hyperparameter vector (λ, α) , and use cross-validation over a grid of hyperparameter values, solving an inequality constrained PLQ for each choice using the techniques in this paper. Now, the model selection process is intuitive, and the entire approach is efficiently implementable, since the number of arithmetic operations required for the evaluation of each choice of hyperparameters is proportional to that of standard RLS approaches. The combination of spline kernel modeling with PLQ optimization paves the way to for a range of new applications of robust and inequality constrained linear system identification.

6.1. Acknowledgements. The authors are grateful to Stephen Becker, for insightful discussions about TFOCS and assistance in implementation of the TFOCS SVR formulation.

7. Appendix.

7.1. Details on data generation in the introductory example. The impulse response displayed in Fig. 1.1 (top panels, continuous line) is the completely monotonic function $f(t) = (t+2)^{-2}$, $t \geq 0$. Consider a discrete-time system whose impulse response is the sampled version of $f(t)$ obtained by adopting a unit sampling time. Then, system output samples are generated applying to this system (initially at rest) an input which is realization from white Gaussian noise of unit variance. Under nominal conditions, the measurement noise is Gaussian with σ^2 equal to the variance of the noiseless output divided by 10. This leads to the data set visible in the bottom left panel of Fig. 1.1. To simulate perturbed conditions, the noise is instead a mixture of two normals with a fraction of outlier contamination equal to 0.1; i.e. $e_i \sim 0.9\mathcal{N}(0, \sigma^2) + 0.1\mathcal{N}(0, 100\sigma^2)$ with σ^2 defined as in the previous case. This leads to the output samples in the bottom right panel of Fig. 1.1. Finally, the impulse response estimates from $SS + L_2$ reported in the top panels (dashdot line) are obtained by the stable spline described in subsection 2.3, using (2.9), (2.10) and setting the dimension of x to 100.

7.2. Computation of the KKT Conditions for Problem (3.4). Let the problem (3.4) be specified by (3.7) and (4.6). Consider the convex function $h : \mathbb{R}^k \times \mathbb{R}^p \rightarrow \bar{\mathbb{R}}$ given by

$$h(z, r) = \sup \left[\langle z, u \rangle - \frac{1}{2} \langle u, Mu \rangle - \delta \left(c - C^T u \mid \mathbb{R}_+^l \right) \right] + \delta \left(r \mid \mathbb{R}_+^l \right).$$

Then, problem (3.4) can be written as the convex composite optimization problem

$$\min_y h(b + By, a - A^T y). \quad (7.1)$$

The convex composite Lagrangian for this problem [15, 16, 72] is given by

$$L(y, u, w) = \left\langle \begin{pmatrix} u \\ w \end{pmatrix}, \begin{pmatrix} b + By \\ a - A^T y \end{pmatrix} \right\rangle - h^*(u, w),$$

where h^* is the convex conjugate of H and is given by

$$h^*(u, w) = \frac{1}{2} \langle u, Mu \rangle + \delta \left(c - C^T u \mid \mathbb{R}_+^l \right) + \delta \left(w \mid \mathbb{R}_-^l \right).$$

The first-order optimality conditions for (7.1), or KKT conditions, can be written as

$$0 \in \partial_y L(y, u, w), 0 \in \partial_u (-L(y, u, w)) \text{ and } 0 \in \partial_w (-L(y, u, w)),$$

where ∂ denotes the subdifferential operator from convex analysis. Since the problem (7.1) is convex and all of the constraints are polyhedral, these conditions are both necessary and sufficient for optimality. By applying the subdifferential calculus [71], the KKT conditions become

$$\begin{aligned}
0 &= C^T u + s - c \\
0 &= A^T y + r - a \\
0 &= By - Mu - Cq + b \\
0 &= B^T u + Aw \\
0 &= q_i s_i \quad \forall i, \quad q, s \geq 0 \\
0 &= w_i r_i \quad \forall i, \quad w, r \geq 0,
\end{aligned} \tag{7.2}$$

where the first two equations define the slack variables $s = c - C^T u$ and $r = a - A^T y$, the third and fourth equations correspond to the inclusions $0 \in \partial_u(-L(y, u, w))$ and $0 \in \partial_y L(y, u, w)$, respectively, and the fifth and sixth equations give the normal cone inclusions $q \in N(s | \mathbb{R}_+^l)$ and $r \in N(w | \mathbb{R}_+^p)$, respectively, with the latter of these equivalent to the inclusion $0 \in \partial_w(-L(y, u, w))$. The normal cone inclusions correspond to the complementarity conditions. These conditions are equivalent to the statement (4.8) which in turn can be reformulated as the MLCP (4.1).

7.3. Proof of Theorem 4.1. The matrix \mathcal{H} in (4.3) is injective if and only if $\text{Nul}(\mathcal{H}) = \{0\}$. This immediately implies the condition (4.4). On the other hand, if (4.4) holds and $(u^T, v^T)^T \in \text{Nul}(\mathcal{H})$, then $u \in \text{Nul}(C^T) \cap \text{Nul}(B^T)$ with $Mu = Bv$. Consequently, $u^T Mu = u^T Bv = 0$ so that $Mu = 0$ since M is symmetric and positive semi-definite. Hence, $u = 0$ by (4.4). Moreover, $0 = Mu = Bv = 0$ which implies that $v = 0$ since B is injective. Therefore, the condition (4.4) implies that $\text{Nul}(\mathcal{H}) = \{0\}$.

7.4. Proof of Theorem 4.2. Given $(u, y) \in \mathbb{R}^k \times \mathbb{R}^n$ and $(q, w, s, r) \in \mathcal{D}_{++}$, and recall that $F_\mu^{(1)}(q, w, u, y, s, r)$ is given by the block structured matrix in (4.9). We row reduce $F_\mu^{(1)}(q, w, u, y, s, r)$ by using the lower right-hand block to eliminate the upper right-hand block and then use the upper left-hand block to eliminate the middle left-hand block to obtain the reduced matrix

$$\left[\begin{array}{cc|cc|cc} S^{-1}Q & 0 & -C^T & 0 & 0 & 0 \\ 0 & R^{-1}W & 0 & -A^T & 0 & 0 \\ \hline 0 & 0 & M + CSQ^{-1}C^T & -B & 0 & 0 \\ 0 & 0 & B^T & ARW^{-1}A^T & 0 & 0 \\ \hline Q & 0 & 0 & 0 & S & 0 \\ 0 & W & 0 & 0 & 0 & R \end{array} \right]. \tag{7.3}$$

Hence $F_\mu^{(1)}(q, w, u, y, s, r)$ is invertible if and only if the matrix (4.10) (the matrix in the central 2×2 block of the reduced matrix above) is invertible. Clearly, by considering the first column of (4.10), the invertibility of (4.10) implies the condition (4.4). We now show the converse. Indeed, if this matrix were not invertible, then there would exist a nonzero $(u, y) \in \mathbb{R}^k \times \mathbb{R}^n$ such that

$$\begin{aligned}
By &= (M + CSQ^{-1}C^T)u \\
B^T u &= -ARW^{-1}A^T y.
\end{aligned}$$

Multiplying the first equation on the left by u and the second on the left by y gives

$$0 \leq u^T (M + CSQ^{-1}C^T)u = u^T By = -y^T ARW^{-1}A^T y \leq 0,$$

and so $u \in \text{Nul}(M) \cap \text{Nul}(C^T)$ and $By = 0$. The injectivity of B gives $y = 0$ so that $B^T u = 0$ with $u \neq 0$ giving $u \in \text{Nul}(M) \cap \text{Nul}(C^T) \cap \text{Nul}(B^T) \neq \{0\}$. Therefore, (4.4) does not hold. This establishes the result.

7.5. Computation of the Newton Step in Algorithm 4.1. To compute the Newton step in Step (2) of of Algorithm 4.1 we make use of the simplifying assumption (4.5) which is satisfied by all of the PLQ functions of current interest.

Let the matrices T and Ω be as given in (4.11) and let \mathcal{G} denote the row reduction matrix that transforms the matrix (4.9) into the matrix (7.3). Setting

$$\begin{pmatrix} \eta_1 \\ \eta_2 \\ \eta_5 \\ \eta_6 \end{pmatrix} := \begin{pmatrix} c - C^T u - s + \mu s^{-1} - q \\ a - A^T r - r + \mu r^{-1} - w \\ \mu \mathbf{1} - Qs \\ \mu \mathbf{1} - Wr \end{pmatrix},$$

and

$$\begin{pmatrix} \eta_3 \\ \eta_4 \end{pmatrix} := \begin{pmatrix} b + By - Mu + C(s - q - \mu q^{-1} - SQ^{-1}\eta_1) \\ -B^T u + A(r - w - \mu w^{-1} - RW^{-1}\eta_2) \end{pmatrix}$$

gives $\mathcal{G}F_\mu = \eta$, where $q^{-1} = Q^{-1}\mathbf{1}$ and $w^{-1} = W^{-1}\mathbf{1}$. Hence, by using the center block in (7.3), we obtain

$$\Delta y = \Omega^{-1}(\eta_4 - B^T \hat{\eta}_3), \quad \Delta u = \hat{\eta}_3 + T^{-1}B\Delta y,$$

where $\hat{\eta}_3 := T^{-1}\eta_3$, which in turn yields

$$\begin{aligned} \Delta q &= Q^{-1}S(\eta_1 + C^T \Delta u), \quad \Delta w = W^{-1}R(\eta_2 + A^T \Delta y) \\ \Delta r &= S^{-1}(\eta_5 - Q\Delta q), \quad \Delta s = R^{-1}(\eta_6 - W\Delta w). \end{aligned}$$

7.6. Proof of Theorem 4.3. The algorithm is implementable under the given hypotheses by Theorem 4.2. The remainder of the proof proceeds by establishing a series of claims. Define

$$\widehat{\mathcal{F}}_+(\tau) := \{(q, w, r, s) \mid \exists (u, w) \text{ s.t. } (q, w, u, y, r, s) \in \mathcal{F}_+(\tau)\}.$$

Claim (i): To each $\tau > 0$ and $(q, w, r, s) \in \widehat{\mathcal{F}}_+(\tau)$ there is a unique (u, y) such that

$$(q, w, u, y, r, s) \in \mathcal{F}_+(\tau)$$

Proof: Suppose (u^i, y^i) are such that $(q, w, u^i, y^i, r, s) \in \mathcal{F}_+(\tau)$ for $i = 1, 2$, and set $u := u^1 - u^2$ and $y := y^1 - y^2$. Then, by (4.1),

$$A^T y = 0, \quad B^T u = 0, \quad C^T u = 0 \text{ and } Mu = By. \quad (7.4)$$

Hence $u^T Mu = u^T By = 0$ so that $Mu = 0$ as M is symmetric positive semi-definite. Therefore, $u = 0$ by the injectivity condition (4.4). In addition, $By = 0$ so that $y = 0$ since B is injective.

Claim (ii): The set $\mathcal{F}_+(\tau)$ is bounded for all $\tau > 0$.

Proof: Let $(q, r, u, y, r, s) \in \mathcal{F}_+(\tau)$ and $(\hat{q}, \hat{r}, \hat{u}, \hat{y}, \hat{r}, \hat{s}) \in \mathcal{F}_+(+\infty)$, then, by (4.1),

$$\begin{aligned} \begin{pmatrix} q - \hat{q} \\ w - \hat{w} \end{pmatrix}^T \begin{pmatrix} s - \hat{s} \\ r - \hat{r} \end{pmatrix} &= (q - \hat{q})^T (s - \hat{s}) + (w - \hat{w})^T (r - \hat{r}) \\ &= (q - \hat{q})^T C^T (\hat{u} - u) + (w - \hat{w})^T A^T (\hat{y} - y) \\ &= (Cq - C\hat{q})^T (\hat{u} - u) + (Aw - A\hat{w})^T (\hat{y} - y) \\ &= (B(y - \hat{y}) - M(u - \hat{u}))^T (\hat{u} - u) + (B(\hat{u} - u))^T (\hat{y} - y) \\ &= (u - \hat{u})^T M(u - \hat{u}) \geq 0. \end{aligned} \quad (7.5)$$

Therefore,

$$\tau + \hat{q}^T \hat{s} + \hat{w}^T \hat{r} \geq q^T \hat{s} + s^T \hat{q} + w^T \hat{r} + r^T \hat{w} \geq \gamma \|(q, r, s, w)\|_1,$$

where $\gamma := \min\{\hat{s}_i, \hat{q}_i, \hat{r}_j, \hat{w}_j : 1 \leq i \leq l, 1 \leq j \leq p\} > 0$, and so $\widehat{\mathcal{F}}_+(\tau)$ is bounded. Consequently, if $\mathcal{F}_+(\tau)$ is unbounded, there is a sequence $\{(q^k, r^k, u^k, y^k, s^k)\} \subset \mathcal{F}_+(\tau)$ with $\{(q^k, r^k, s^k)\}$ bounded and $\{(u^k, y^k)\}$ unbounded. With no loss in generality,

$$(u^k, y^k) / \|u^k, y^k\| \rightarrow (u, y) \neq (0, 0).$$

Dividing (4.1) by $\|u^k, y^k\|$ and taking the limit gives (7.4) which implies that $(u, y) = (0, 0)$, a contradiction. Hence, $\mathcal{F}_+(\tau)$ is bounded.

Claim (iii): The set $\mathcal{F}_+(\tau)$ is convex for all $\tau > 0$.

Proof: By (4.1), for every $(q, r, u, y, r, s) \in \mathcal{F}_+(\tau)$ we have

$$\begin{aligned} q^T s + w^T r &= q^T (c - C^T u) + w^T (a - A^T y) \\ &= c^T q - u^T C q + a^T w - y^T A w \\ &= c^T q + a^T w + u^T (Mu - By - b) + u^T B y \\ &= c^T q + a^T w - b^T u + u^T M u, \end{aligned}$$

where the final expression is a convex function ψ in (q, r, u, y, r, s) . Hence, the set $\mathcal{F}_+(\tau)$ is the intersection of the affine set defined by (4.1), the convex set $\{(q, r, u, y, r, s) : \psi(q, r, u, y, r, s) \leq \tau\}$, and the set $\mathbb{R}_{++}^l \times \mathbb{R}_{++}^p \times \mathbb{R}^k \times \mathbb{R}^n \times \mathbb{R}_{++}^p \times \mathbb{R}_{++}^l$, and is therefore convex.

Claim (iv): For every $v \in \mathbb{R}_{++}^l$ and $\omega \in \mathbb{R}_{++}^p$ there exists a unique $(q, w, r, s) \in \widehat{\mathcal{F}}_+(\infty)$ such that $Qs = v$ and $Wr = \omega$.

Proof: We first show existence. Let $(\hat{q}, \hat{r}, \hat{u}, \hat{y}, \hat{r}, \hat{s}) \in \widehat{\mathcal{F}}_+(\infty)$, $v \in \mathbb{R}_{++}^l$, and $\omega \in \mathbb{R}_{++}^p$, and set $\hat{v} := \hat{Q}\hat{s} \in \mathbb{R}_{++}^l$ and $\hat{\omega} := \hat{W}\hat{r} \in \mathbb{R}_{++}^p$. Define

$$F(q, w, u, y, s, r, t) := \begin{pmatrix} C^T u + s - c \\ A^T y + r - a \\ Mu + Cq - By - b \\ B^T u + Aw \\ Qs - ((1-t)\hat{v} + tv) \\ Wr - ((1-t)\hat{\omega} + t\omega) \end{pmatrix}. \quad (7.6)$$

Note that $F(\hat{q}, \hat{r}, \hat{u}, \hat{y}, \hat{r}, \hat{s}, 0) = 0$ and, by Theorem 4.2, $\nabla_{(q, w, u, y, s, r)} F(\hat{q}, \hat{r}, \hat{u}, \hat{y}, \hat{r}, \hat{s}, 0)^{-1}$ exists. The Implicit Function Theorem implies that there is a $\hat{t} > 0$ and a differentiable mapping $(q(t), w(t), u(t), y(t), s(t), r(t))$ on $[0, \hat{t})$ such that $F(q(t), w(t), u(t), y(t), s(t), r(t), t) = 0$ on $[0, \hat{t})$. Let \bar{t} be the largest such \hat{t} on $(0, 1]$. Since $\{(q(t), w(t), u(t), y(t), s(t), r(t)) : t \in [0, \bar{t})\} \subset \widehat{\mathcal{F}}_+(\bar{\tau})$, where $\bar{\tau} = \max\{\mathbf{1}^T v + \mathbf{1}^T \omega, \mathbf{1}^T \hat{v} + \mathbf{1}^T \hat{\omega}\}$, Claim (ii) implies that there is a sequence $t_k \uparrow \bar{t}$ and a point $(\bar{q}, \bar{r}, \bar{u}, \bar{y}, \bar{r}, \bar{s})$ such that $(q(t_k), w(t_k), u(t_k), y(t_k), s(t_k), r(t_k)) \rightarrow (\bar{q}, \bar{r}, \bar{u}, \bar{y}, \bar{r}, \bar{s})$, where, by continuity, $F(\bar{q}, \bar{r}, \bar{u}, \bar{y}, \bar{r}, \bar{s}, \bar{t}) = 0$. If $\bar{t} = 1$, we are done; otherwise, apply the Implicit Function Theorem again at $(\bar{q}, \bar{r}, \bar{u}, \bar{y}, \bar{r}, \bar{s}, \bar{t})$ to obtain a contradiction to the maximality of \bar{t} .

We now show uniqueness. By Claim (i), we need only establish the uniqueness of (q, w, r, s) . Let $(q^k, w^k, r^k, s^k) \in \widehat{\mathcal{F}}_+(\infty)$, be such that $Q_k s^k = v$ and $W_k r^k = \omega$, $k = 1, 2$. Set $\xi^k := (q^k, w^k)$ and $\zeta^k := (s^k, r^k)$, $k = 1, 2$, and $\alpha = (v, \omega)$. By (7.5), $0 \leq (\xi^1 - \xi^2)^T (\zeta^1 - \zeta^2)$. If $(\xi^1, \zeta^1) \neq (\xi^2, \zeta^2)$, then, for some $i \in \{1, 2, \dots, l+p\}$, $(\xi_i^1 - \xi_i^2)^T (\zeta_i^1 - \zeta_i^2) \geq 0$ and either $\xi_i^1 \neq \xi_i^2$ or $\zeta_i^1 \neq \zeta_i^2$. If $\xi_i^1 > \xi_i^2$, then $\zeta_i^1 \geq \zeta_i^2 > 0$, so $\alpha_i = \xi_i^1 \zeta_i^1 > \xi_i^2 \zeta_i^2 = \alpha_i$, a

contradiction. So with no loss in generality (by exchanging (ξ^1, ζ^1) with (ξ^2, ζ^2) if necessary), we must have $\zeta_i^1 > \zeta_i^2$. But then $\xi_i^1 \geq \xi_i^2 > 0$ so that again we have the contradiction $\alpha_i = \xi_i^1 \zeta_i^1 > \xi_i^2 \zeta_i^2 = \alpha_i$. Therefore, (q, w, r, s) is unique.

The proof of Theorem 4.3 follows easily from Claims (i)-(iv). Claim (iv) shows that the Central Path is well defined for $\tau > 0$ by taking $v := \mu \mathbf{1}$ and $w := \mu \mathbf{1}$. By Claim (ii), cluster points for the Central Path must exist as $\mu \downarrow 0$, and, by continuity, all of them must be KKT points for (3.7).

7.7. Proof of Theorem 4.4. Note that if C has on the order of k entries, the matrix T can be constructed in $O(l + k)$ operations. If T is diagonal, building $B^T T^{-1} B$ takes $O(n^2 k)$ operations. The matrix ADA^T can be formed in $O(pn^2)$ operations in general, and in $O(n)$ operations when A has on the order of n entries. Also, Ω is in $\mathbb{R}^{n \times n}$, so can be inverted in $O(n^3)$ operations. These operations dominate the complexity, giving the worst case bound $O((p + k + n)n^2)$, under the assumptions on C and T .

7.8. Proof of Corollary 4.5. To translate (3.4) to (3.7), we have to specify the structures A, B, b, C, c , which capture the impulse response constraints, the injective linear model, and the structure of U , respectively.

Suppose that $\rho_w(y)$ and $\rho_v(x)$ are given by

$$\begin{aligned}\rho_w(y) &:= \sup_{u \in U_w} \langle b_w + B_w y, u \rangle - \frac{1}{2} u^T M_w u \\ \rho_v(x) &:= \sup_{u \in U_v} \langle b_v + B_v x, u \rangle - \frac{1}{2} u^T M_v u\end{aligned}\tag{7.7}$$

First define

$$\begin{aligned}\tilde{\rho}_v(y) &:= \rho_v(\gamma^{-1}(\Phi L y - z)) \\ &= \sup_{u \in U_v} \langle b_v - \gamma^{-1} B_v z + \gamma^{-1} B_v \Phi L y, u \rangle - \frac{1}{2} u^T M_v u.\end{aligned}$$

Adding $\tilde{\rho}_v$ and ρ_w together, we obtain the general system identification objective with the following specification:

$$\begin{aligned}M &= \begin{bmatrix} M_w & 0 \\ 0 & M_v \end{bmatrix}, \quad B = \begin{bmatrix} B_w \\ \gamma^{-1} B_v \Phi L \end{bmatrix}, \quad b = \begin{bmatrix} b_w \\ b_v - \gamma^{-1} B_v z \end{bmatrix} \\ C &= \begin{bmatrix} C_w & 0 \\ 0 & C_v \end{bmatrix}, \quad c = \begin{bmatrix} c_w \\ c_v \end{bmatrix}.\end{aligned}$$

The matrix A and vector a encodes the constraints, as given by (3.7). This completes the specification. The complexity result follows immediately from the assumptions on A, B, C and Theorem 4.4.

It is also worthwhile to consider the structure of the Newton step in Algorithm 4.1. First, note that

$$\begin{aligned}T &= M + C Q S^{-1} C^T \\ &= \begin{bmatrix} M_w & 0 \\ 0 & M_v \end{bmatrix} + \begin{bmatrix} C_w & 0 \\ 0 & C_v \end{bmatrix} Q S^{-1} \begin{bmatrix} C_w & 0 \\ 0 & C_v \end{bmatrix}^T \\ &= \begin{bmatrix} M_w + C_w Q_w S_w^{-1} C_w^T & 0 \\ 0 & M_v + C_v Q_v S_v^{-1} C_v^T \end{bmatrix} \\ &= \begin{bmatrix} T_w & 0 \\ 0 & T_v \end{bmatrix},\end{aligned}$$

so T is block diagonal. This fact gives a more explicit formula for Ω :

$$\begin{aligned}\Omega &= B^T T^{-1} B + A R^{-1} W A^T \\ &= \begin{bmatrix} B_w^T & \gamma^{-1} L^T \Phi^T B_v^T \end{bmatrix} \begin{bmatrix} T_w^{-1} & 0 \\ 0 & T_v^{-1} \end{bmatrix} \begin{bmatrix} B_w \\ \gamma^{-1} B_v \Phi L \end{bmatrix} + A R^{-1} W A^T \\ &= B_w^T T_w^{-1} B_w + \sigma^{-2} L^T \Phi^T B_v^T T_v^{-1} B_v \Phi L + A R^{-1} W A^T .\end{aligned}$$

If A is sparse and $K \sim O(n+m)$, Ω can be formed and inverted in $n^2(m+n)$ operations, linear in m as claimed.

REFERENCES

- [1] A. Aravkin, P. Kambadur, A. Lozano, and R. Luss. Orthogonal matching pursuit for sparse quantile regression. In *Data Mining (ICDM), International Conference on*, pages 11–19. IEEE, 2014.
- [2] H. Akaike. A new look at the statistical model identification. *IEEE Transactions on Automatic Control*, 19:716–723, 1974.
- [3] M. Antinescu, G. Lesaja, and F. Potra. Equivalence between different formulations of the linear complementary problem. *Optimization Methods and Software*, 7:265–290, 1997.
- [4] A. Aravkin, B. M. Bell, J. V. Burke, and G. Pillonetto. An ℓ_1 -Laplace robust Kalman smoother. *IEEE Transactions on Automatic Control*, 56(12):2898–2911, 2011.
- [5] A. Aravkin, B. M. Bell, J. V. Burke, and G. Pillonetto. Learning Using State Space Kernel Machines. In *Proc. IFAC World Congress 2011*, Milan, Italy, 2011.
- [6] A. Aravkin, J. Burke, A. Chiuso, and G. Pillonetto. Convex vs non-convex estimators for regression and sparse estimation: the mean squared error properties of ard and glasso. *Journal of Machine Learning Research*, 15:217–252, 2014.
- [7] A. Aravkin, J. Burke, and G. Pillonetto. A statistical and computational theory for robust and sparse Kalman smoothing. In *Proceedings of the 16th IFAC Symposium on System Identification (SysId 2012)*, 2012.
- [8] A. Aravkin, J. V. Burke, and G. Pillonetto. Linear system identification using stable spline kernels and plq penalties. To appear in *IEEE Conf. Decision and Control (CDC), March 2013*, 2013.
- [9] A. Aravkin, J. V. Burke, and G. Pillonetto. Sparse/robust estimation and kalman smoothing with nonsmooth log-concave densities: Modeling, computation, and theory. *Journal of Machine Learning Research*, 14:2689–2728, 2013.
- [10] S. Becker, E. Candes, and M. Grant. Templates for convex cone problems with applications to sparse signal recovery. *Mathematical Programming Computation*, 3(3):165–218, 2011.
- [11] J. Berger. *Statistical Decision Theory and Bayesian Analysis*. Springer Series in Statistics. Springer, second edition, 1985.
- [12] M. Bertero. Linear inverse and ill-posed problems. *Advances in Electronics and Electron Physics*, 75:1–120, 1989.
- [13] K. Bube and T. Nemeth. Fast line searches for the robust solution of linear systems in the hybrid ℓ_1/ℓ_2 and huber norms. *Geophysics*, 72(2):A13–A17, 2007.
- [14] M. Buchinsky. Changes in the u.s. wage structure 1963-1987: Application of quantile regression. *Econometrica*, 62(2):405–58, March 1994.
- [15] J. Burke. Second order necessary and sufficient conditions for convex composite NDO. *Mathematical programming*, 38(3):287–302, 1987.
- [16] J. Burke and R. Poliquin. Optimality conditions for non-finite valued convex composite functions. *Mathematical Programming*, 57(1):103–120, 1992.
- [17] C.-C. Chang and C.-J. Lin. Libsvm: a library for support vector machines. *ACM Transactions on Intelligent Systems and Technology (TIST)*, 2(3):27, 2011.
- [18] T. Chen, H. Ohlsson, G. Goodwin, and L. Ljung. Kernel selection in linear system identification – part II: A classical perspective. In *Proceedings of CDC-ECC*, 2011.
- [19] T. Chen, H. Ohlsson, and L. Ljung. On the estimation of transfer functions, regularizations and Gaussian processes - revisited. *Automatica*, 48(8):1525–1535, 2012.
- [20] W. Chu, S. S. Keerthi, and C. J. Ong. A unified loss function in bayesian framework for support vector regression. *Epsilon*, 1(1.5):2, 2001.
- [21] D. Clark. The mathematical structure of huber’s m-estimator. *SIAM Journal on Scientific and Statistical Computing*, 6:1:209–219, 1985.
- [22] F. Cucker and S. Smale. On the mathematical foundations of learning. *Bulletin of the American Mathematical Society*, 39:1–49, 2001.

- [23] C. De Mol, E. De Vito, and L. Rosasco. Elastic-net regularization in learning theory. *Journal of Complexity*, 25(2):201–230, 2009.
- [24] O. Dekel, S. Shalev-Shwartz, and Y. Singer. Smooth epsilon-insensitive regression by loss symmetrization. In *Journal of Machine Learning Research*, pages 711–741, 2005.
- [25] D. Donoho. Compressed sensing. *IEEE Trans. on Information Theory*, 52(4):1289–1306, 2006.
- [26] R. Dutter and P. J. Huber. Numerical Methods for the Nonlinear Robust Regression Problem. *Journal of Statistical Computation and Simulation*, 13:79–113, 1981.
- [27] B. Efron, T. Hastie, L. Johnstone, and R. Tibshirani. Least angle regression. *Annals of Statistics*, 32:407–499, 2004.
- [28] T. Evgeniou, M. Pontil, and T. Poggio. Regularization networks and support vector machines. *Advances in Computational Mathematics*, 13:1–150, 2000.
- [29] S. Farahmand, G. B. Giannakis, and D. Angelosante. Doubly Robust Smoothing of Dynamical Processes via Outlier Sparsity Constraints. *IEEE Transactions on Signal Processing*, 59:4529–4543, 2011.
- [30] D. A. Freedman. *Statistical models: theory and practice*. cambridge university press, 2009.
- [31] J. Gao. Robust l1 principal component analysis and its {B}ayesian variational inference. *Neural Computation*, 20(2):555–572, Feb. 2008.
- [32] F. Girosi. Models of noise and robust estimates. A.I. Memo 1287, Artificial Intelligence Laboratory, 1287, Massachusetts Institute of Technology, 1991.
- [33] G. Goodwin, M. Gevers, and B. Ninness. Quantifying the error in estimated transfer functions with application to model order selection. *IEEE Transactions on Automatic Control*, 37(7):913–928, 1992.
- [34] M. Grant and S. Boyd. Graph implementations for nonsmooth convex programs. In V. Blondel, S. Boyd, and H. Kimura, editors, *Recent Advances in Learning and Control*, Lecture Notes in Control and Information Sciences, pages 95–110. Springer-Verlag Limited, 2008. http://stanford.edu/~boyd/graph_dcp.html.
- [35] M. Grant and S. Boyd. CVX: Matlab software for disciplined convex programming, version 2.1. <http://cvxr.com/cvx>, Mar. 2014.
- [36] O. Güler. Generalized linear complementarity problems. *Mathematics of Operations Research*, 20:441–448, 1995.
- [37] T. Hastie and R. Tibshirani. Generalized additive models. In *Monographs on Statistics and Applied Probability*, volume 43. Chapman and Hall, London, UK, 1990.
- [38] T. Hastie, R. Tibshirani, and J. Friedman. *The Elements of Statistical Learning. Data Mining, Inference and Prediction*. Springer, Canada, 2001.
- [39] F. Herrmann, M. Friedlander, and O. Yilmaz. Fighting the curse of dimensionality: Compressive sensing in exploration seismology. *Signal Processing Magazine, IEEE*, 29(3):88–100, 2012.
- [40] F. J. Herrmann and G. Hennenfent. Non-parametric seismic data recovery with curvelet frames. *Geophysical Journal International*, 173(1):233–248, 2008.
- [41] P. J. Huber. *Robust Statistics*. John Wiley and Sons, 2004.
- [42] C. Hurvich and C. Tsai. Regression and time series model selection in small samples. *Biometrika*, 76:297–307, 1989.
- [43] R. Koenker. *Quantile Regression*. Cambridge University Press, 2005.
- [44] R. Koenker and G. Bassett. Regression quantiles. *Econometrica*, pages 33–50, 1978.
- [45] R. Koenker and O. Geling. Reappraising medfly longevity: A quantile regression survival analysis. *Journal of the American Statistical Association*, 96:458468, 2001.
- [46] R. Koenker and K. F. Hallock. Quantile regression. *Journal of Economic Perspectives, American Economic Association*, pages 143–156, 2001.
- [47] M. Kojima, N. Megiddo, T. Noma, and A. Yoshise. *A Unified Approach to Interior Point Algorithms for Linear Complementarity Problems*, volume 538 of *Lecture Notes in Computer Science*. Springer Verlag, Berlin, Germany, 1991.
- [48] Y.-J. Lee, W.-F. Hsieh, and C.-M. Huang. ϵ -ssvr: a smooth support vector machine for ϵ -insensitive regression. *Knowledge and Data Engineering, IEEE Transactions on*, 17(5):678–685, 2005.
- [49] Y.-J. Lee and O. L. Mangasarian. Ssvm: A smooth support vector machine for classification. *Computational optimization and Applications*, 20(1):5–22, 2001.
- [50] Q. Li, N. Lin, et al. The bayesian elastic net. *Bayesian Analysis*, 5(1):151–170, 2010.
- [51] W. Li and J. Swetits. The linear l1 estimator and the huber m-estimator. *SIAM Journal on Optimization*, 8(2):457–475, 1998.
- [52] L. Ljung. *System Identification, Theory for the User*. Prentice Hall, 1999.
- [53] D. MacKay. Bayesian interpolation. *Neural Computation*, 4:415–447, 1992.
- [54] J. Mairal, M. Elad, and G. Sapiro. Sparse representation for color image restoration. *IEEE Transactions on Image Processing*, 17(1):53–69, Jan. 2008.
- [55] H. Mansour, R. Saab, P. Nasiopoulos, and R. Ward. Color image desaturation using sparse reconstruction. In *Proc. of the IEEE International Conference on Acoustics, Speech, and Signal Processing (ICASSP)*, pages 778–781, March 2010.

- [56] H. Mansour, H. Wason, T. T. Y. Lin, and F. J. Herrmann. Randomized marine acquisition with compressive sampling matrices. *Geophysical Prospecting*, 60(4):648–662, 2012.
- [57] J. S. Maritz and T. Lwin. *Empirical Bayes Method*. Chapman and Hall, 1989.
- [58] R. A. Maronna, D. Martin, and Yohai. *Robust Statistics*. Wiley Series in Probability and Statistics. Wiley, 2006.
- [59] R. Neelamani, C. Krohn, J. Krebs, J. Romberg, M. Deffenbaugh, and J. Anderson. Efficient seismic forward modeling using simultaneous random sources and sparsity. *Geophysics*, 75(6):WB15–WB27, 2010.
- [60] A. Nemirovskii and Y. Nesterov. *Interior-Point Polynomial Algorithms in Convex Programming*, volume 13 of *Studies in Applied Mathematics*. SIAM, Philadelphia, PA, USA, 1994.
- [61] Y. Nesterov. A method for solving the convex programming problem with convergence rate $O(1/k^2)$. *Dokl. Akad. Nauk SSSR*, 269(3):543–547, 1983.
- [62] Y. Nesterov. Smooth minimization of non-smooth functions. *Mathematical programming*, 103(1):127–152, 2005.
- [63] G. Pillonetto, A. Chiuso, and G. De Nicolao. Regularized estimation of sums of exponentials in spaces generated by stable spline kernels. In *Proceedings of the IEEE American Cont. Conf., Baltimora, USA*, 2010.
- [64] G. Pillonetto, A. Chiuso, and G. D. Nicolao. Prediction error identification of linear systems: a nonparametric Gaussian regression approach. *Automatica*, 47(2):291–305, 2011.
- [65] G. Pillonetto and G. De Nicolao. A new kernel-based approach for linear system identification. *Automatica*, 46(1):81–93, 2010.
- [66] G. Pillonetto and G. De Nicolao. Kernel selection in linear system identification – part I: A Gaussian process perspective. In *Proceedings of CDC-ECC*, 2011.
- [67] G. Pillonetto and G. De Nicolao. Pitfalls of the parametric approaches exploiting cross-validation or model order selection. In *Proceedings of the 16th IFAC Symposium on System Identification (SysId 2012)*, 2012.
- [68] G. Pillonetto, F. Dinuzzo, T. Chen, G. D. Nicolao, and L. Ljung. Kernel methods in system identification, machine learning and function estimation: a survey. *Automatica*, March, 2014.
- [69] M. Pontil and A. Verri. Properties of support vector machines. *Neural Computation*, 10:955–974, 1998.
- [70] C. Rasmussen and C. Williams. *Gaussian Processes for Machine Learning*. The MIT Press, 2006.
- [71] R. T. Rockafellar and R. T. Rockafellar. *Convex Analysis*. Princeton Landmarks in Mathematics. Princeton University Press, 1970.
- [72] R. T. Rockafellar and R. J. B. Wets. *Variational Analysis*, volume 317. Springer, 1998.
- [73] B. Schölkopf, A. Smola, R. Williamson, and P. Bartlett. New support vector algorithms. *Neural Computation*, 12:1207–1245, 2000.
- [74] B. Schölkopf and A. J. Smola. *Learning with Kernels: Support Vector Machines, Regularization, Optimization, and Beyond*. (Adaptive Computation and Machine Learning). MIT Press, 2001.
- [75] G. Schwarz et al. Estimating the dimension of a model. *The annals of statistics*, 6(2):461–464, 1978.
- [76] G. Seber and C. Wild. *Nonlinear Regression*. Wiley Series in Probability and Statistics. Wiley, 2003.
- [77] T. Söderström and P. Stoica. *System Identification*. Prentice-Hall, 1989.
- [78] J.-L. Starck, M. Elad, and D. Donoho. Image decomposition via the combination of sparse representation and a variational approach. *IEEE Transaction on Image Processing*, 14(10), 2005.
- [79] R. Tibshirani. Regression shrinkage and selection via the LASSO. *Journal of the Royal Statistical Society, Series B.*, 58(1):267–288, 1996.
- [80] A. Tikhonov. *Numerical methods for the solution of ill-posed problems*.
- [81] V. Vapnik. *Statistical Learning Theory*. Wiley, New York, NY, USA, 1998.
- [82] J. C. Willems. Dissipative dynamical systems. part II: Linear systems with quadratic supply rates. *Archive for Rational Mechanics and Analysis*, 45(5):352–393, 1972.
- [83] S. Wright. A path-following interior point algorithm for linear and quadratic problems. *Annals of Operations Research*, 62:103–130, 1996.
- [84] S. J. Wright. *Primal-Dual Interior-Point Methods*. Siam, Englewood Cliffs, N.J., USA, 1997.
- [85] F. Zanderigo, A. Bertoldo, G. Pillonetto, and C. Cobelli. Nonlinear stochastic regularization to characterize tissue residue function in bolus-tracking mri: Assessment and comparison with svd, block-circulant svd, and tikhonov. *IEEE Transactions on Biomedical Engineering*, 56(5):1287–1297, 2009.
- [86] K. Zierler. Equations for measuring blood flow by external monitoring of radioisotopes. *Circ. Res.*, 16:309–321, 1965.
- [87] H. Zou and T. Hastie. Regularization and variable selection via the elastic net. *Journal of the Royal Statistical Society, Series B*, 67:301–320, 2005.
- [88] H. Zou and T. Hastie. Regularization and variable selection via the elastic net. *Journal of the Royal Statistical Society: Series B (Statistical Methodology)*, 67(2):301–320, 2005.
- [89] H. Zou and M. Yuan. Regularized simultaneous model selection in multiple quantiles regression. *Computational Statistics & Data Analysis*, 52(12):5296–5304, 2008.